

**Please cite the Published Version**

Beake, BD , Roberts, J, Zhu, Y  and Liskiewicz, TW  (2025) Simulating erosion tests with statistically distributed micro-scale impact: a study on PVD TiAlN and AlCrN coatings. *Wear*. 205911 ISSN 0043-1648

**DOI:** <https://doi.org/10.1016/j.wear.2025.205911>

**Publisher:** Elsevier BV

**Version:** Accepted Version

**Downloaded from:** <https://e-space.mmu.ac.uk/638626/>

**Usage rights:**  [Creative Commons: Attribution 4.0](https://creativecommons.org/licenses/by/4.0/)

**Additional Information:** This is an author-produced version of the published paper. Uploaded in accordance with the University's Research Publications Policy

**Enquiries:**

If you have questions about this document, contact [openresearch@mmu.ac.uk](mailto:openresearch@mmu.ac.uk). Please include the URL of the record in e-space. If you believe that your, or a third party's rights have been compromised through this document please see our Take Down policy (available from <https://www.mmu.ac.uk/library/using-the-library/policies-and-guidelines>)

**Simulating erosion tests with statistically distributed micro-scale impact: a study on  
PVD TiAlN and AlCrN coatings**

Ben D. Beake<sup>1,\*</sup>, Josh Roberts<sup>1</sup>, Yibing Zhu<sup>2</sup> and Tomasz W. Liskiewicz<sup>2</sup>

1 Micro Materials Ltd., Willow House, Yale Business Village, Ellice Way, Wrexham, LL13  
7YL, UK

2 John Dalton Building, Faculty of Science and Engineering, Manchester Metropolitan  
University, Chester Street, Manchester M15 6BH, UK

\*Corresponding author: Tel: +44 1978 261615 (B.D. Beake); e-mail:

ben.beake@micromaterials.co.uk (B.D. Beake)

**Abstract**

A novel test method for more closely replicating the statistical, and apparently stochastic, distribution of multiple impacts that occur in solid particle erosion is to perform multiple impacts with controlled energy at different locations on the sample surface using a nanomechanical test instrument where sample stage movement between impacts enables each impact to be at a new position.

In this work we have applied the new method to investigate the behaviour of hard, wear resistant PVD TiAlN and AlCrN coatings on cemented carbide, comparing their behaviour to that in cyclic micro-impact tests where the multiple impacts occur at the same position. Both coatings showed a strongly load-dependent behaviour in the statistically distributed impact test. A transition to lateral cracking with continued impact occurred more readily on AlCrN, with more extensive lateral cracking at higher load than on TiAlN. In contrast, in cyclic impact tests the TiAlN performed poorly at lower load whilst the AlCrN was resistant to

lateral cracking. At high load AlCrN was more variable, with dramatic failure in some tests and no failure in others. Reasons for these differences are discussed.

Keywords: Erosion, impact, PVD, TiAlN, AlCrN.

## 1. Introduction

PVD coatings have been applied to protect components that are subject to solid particle erosion in service, e.g. on compressors in gas turbine engines operating in sandy environments [1-5]. To aid the development of coating systems with improved resistance to solid particle erosion, high velocity erosion tests can be performed, however these tests are time consuming and only provide indirect information about the erosion mechanism. An alternative approach is to complement these tests with rapid small-scale laboratory tests such as cyclic impact tests under controlled conditions which have potential for effective coatings screening. Quantified data is obtained rapidly offering an opportunity to increase the rate of coating development. In many cases behaviour in these tests has shown excellent correlation to performance in actual applications involving repetitive contact, such as in interrupted metal cutting operations, or to solid particle erosion tests, particularly for nano- and micro-scale impact tests with small contact sizes/high pressure contacts [6-13]. However, in a cyclic impact test the repetitive contact occurs at the same position which is not the same as in a real erosive wear where there is a statistical distribution of contacts over a surface. To be better integrated in coatings/surface optimisation campaign it is desirable that the tests can even more closely simulate the actual contact conditions.

The randomised (or statistically distributed) impact test has been developed [14-15] as more direct way to experimentally simulate the stochastic multiple contact nature of erosion by performing repetitive impacts with controlled energy at different locations on the sample

surface using a nanomechanical test instrument where sample stage movement between impacts enables each impact to be at a new position. Figure 1 illustrates typical programmed Gaussian (where there is greater probability of an impact occurring towards the center of the set region) and rectangular (where there is equal probability of an impact occurring anywhere within a set region) distributions of impacts. The figure shows the plastically deformed impact craters as circles which overlap when the impacts are closely spaced. The actual extent of overlap between the impacts is dependent not only on the chosen distribution but on the mechanical properties of the sample and test probe, the test probe geometry and the impact energies.

The novel nano-/micro-scale test method uses probes with radii in the range of a few  $\mu\text{m}$  or less rather than several mm to provide a direct and highly controlled way to better understand microstructural and crack morphological influences on damage propagation at the single-impact level. It has been shown to be more effective than cyclic impact in replicating damage mechanisms and material ranking in erosion tests on glasses [15]. In statistically distributed micro-impact tests on glasses differences in the crack systems that develop under spherical impact were shown with predominantly radial-lateral cracking on BK7 glass and cone cracking on fused silica [15]. Experiments with controlled impact spacing showed that the radial-lateral system has a higher “critical interaction spacing” so that impacts spaced further apart interact causing greater material removal and a more rapid erosion rate for BK7. Cyclic and spatially distributed micro-impact tests on columnar EB-PVD ceramic thermal barrier coating systems with yttria stabilised zirconia (YSZ) and gadolinium zirconate (GZO) topcoats were able to replicate the main mechanisms and surface morphology in solid particle erosion tests [16].

Although cyclic nano- and micro-impact tests have been successful in showing strong correlation to performance of PVD coatings in metal cutting [9-13,17] and statistically distributed micro-impact tests have shown correlation to erosion behaviour for ceramic thermal

barrier coatings [15,16], the statistically distributed impact test has not previously been applied to hard PVD coatings. It is of interest to determine the sensitivity of the technique and its potential for simulating the erosive wear of hard PVD coatings, which is currently studied by classical erosion tests that have some limitations in terms of their repeatability, extended duration and the fact that the progression of the surface erosion can usually only be determined by periodically stopping the test. The statistically distributed test may offer a convenient alternative for coating screening where rapid tests can be performed easily on a wide range of coating compositions, and the progression of the damage monitored impact-by-impact. In this current study the potential of the test is investigated by testing on two well characterised commercial hard PVD nitrides on cemented carbide, TiAlN and AlCrN [17-20]. The coating behaviour in statistically distributed micro-impact has been compared to that in cyclic micro-impact tests, using diamond test probes with end radii 18 and 25  $\mu\text{m}$ . To assess the influence of applied load independently of distribution tests were performed with exactly the same statistical distribution of impacts over a wide load range. To investigate the influence of distribution, tests at higher load were performed with Gaussian and rectangular distributions. The correlation between changing impact depth and energy dissipation during the cyclic and distributed tests was also explored.

## **2. Experimental**

### *2.1 Coatings and nanoindentation*

TiAlN and AlCrN PVD coatings were supplied by the McMaster Manufacturing Research Institute (McMaster University, Hamilton, Canada). The **commercial** coatings were deposited in a standard Balzers RCS cathodic arc coating machine on mirror polished Sandvik H1P cemented carbide inserts to a target 3  $\mu\text{m}$  thickness. Actual coating thickness determined by

calo-wear was 1.7  $\mu\text{m}$  for the TiAlN and 2.5  $\mu\text{m}$  for the AlCrN. There was a  $\sim 200$  nm interlayer in the TiAlN. The Al to Ti ratio is 0.5 in TiAlN (Balinit X.treme), and the Al to Cr ratio is 0.7 in AlCrN (Balinit Alcrona). The columnar coatings have a cubic structure with compressive residual stress of -3 in AlCrN to -4 GPa in TiAlN. The chemical composition of the cemented carbide substrate was 85.5 wt.% WC, 7.5 wt.% TiC, 1.0 wt.% TaC and 6.0 wt.% Co.

Nanomechanical properties were determined with a NanoTest Vantage system (Micro Materials Ltd., Wrexham, UK) under normal laboratory conditions ( $T \sim 22$  °C; RH  $\sim 50\%$ ) using a diamond Berkovich indenter. Instrument and indenter calibration was performed in accordance with ISO14577 [21]. Due to the high surface roughness calotte wear craters were performed in each coating and the nanoindentation tests performed in the worn (smooth) regions. 25 nanoindentation tests were performed on each coating to 30 mN loading/unloading rate = 6 mN/s with a 1 s hold at peak load. These conditions resulted in contact depths close to 150 nm for both coatings.

## 2.2 Cyclic micro-impact tests

For each impact in the micro-impact tests the diamond indenter is withdrawn to a set distance above the sample surface and then rapidly accelerated to produce a high strain rate impact event. The impact energy and effective impact force can be controlled by varying the static load and/or the accelerating distance. For cyclic impact tests, once the probe has come to rest it is retracted and reaccelerated to produce a pre-defined number of cyclic impacts at the same position on the surface. The impacts occur horizontally minimising the amount of debris remaining in the impact crater. Dynamic forces in impact are significantly higher than the set forces. For convenience the tests are described below using the set applied load.

Cyclic micro-impact tests at the same position were performed with the same instrument using two calibrated spheroconical diamond probes (Synton-MDP Ltd, Nidau, Switzerland) with 18 and 25  $\mu\text{m}$  end radii and  $90^\circ$  cone angle impacting at  $90^\circ$  to the surface. The sphere-to-cone transition depths are 5.3  $\mu\text{m}$  and 7.3  $\mu\text{m}$  for the 18 and 25  $\mu\text{m}$  radii probes respectively. The applied loads and accelerating distances in the tests are summarised in Table 1 below. The 75 cycle tests were repeated 15 times at each load. The 500 cycle tests were repeated 3 times at each load at 250, 500 and 750 mN on TiAlN. On AlCrN they were repeated twice at 1000 mN and 3 times at 500 and 750 mN.

**Table 1. Cyclic micro-impact conditions**

$R$ ( $\mu\text{m}$ )	Load (mN)	Acceleration distance ( $\mu\text{m}$ )	Cycles
25	2000, 2500	18	75
18	250, 500, 750, 1000, 1250 1500	50	500

### 2.3 Statistically distributed micro-impact tests

Randomised (statistically distributed) micro-impact tests at  $90^\circ$  were set up using the same two spheroconical diamond probes used for the cyclic impact tests. In all the tests there were 50 statistically distributed impacts within defined regions of the coating surfaces. The applied loads, accelerating distances and distributions used in the tests are summarised in Table 2 below. The same Gaussian distribution was used for all the tests with the 25  $\mu\text{m}$  probe at 500, 1000, 1500 and 2000 mN. Repeat tests with different distributions were performed at 2500 mN. Tests with the 25  $\mu\text{m}$  probe were performed at 2500 mN on both coatings and on AlCrN at 3000 mN with programmed Gaussian and rectangular (i.e. equal probability of impacting

anywhere within the test region) distributions. After the tests the geometry of both probes was rechecked by spherical indentation to confirm that no discernible probe wear had occurred.

**Table 2. Statistically distributed micro-impact conditions**

$R$ ( $\mu\text{m}$ )	Load (mN)	Acceleration distance ( $\mu\text{m}$ )	Impacts	Distribution
25	500, 1000, 1500, 2000, 2500, 3000	18	50	Gaussian within 200 $\mu\text{m}$ x 200 $\mu\text{m}$
25	2500, 3000	18	50	Rectangular within 200 $\mu\text{m}$ x 200 $\mu\text{m}$
18	500, 750, 1000	50	50	Gaussian within 150 $\mu\text{m}$ x 150 $\mu\text{m}$

Each impact in the statistically distributed impact tests was analysed in the instrument software to determine the contact point, the maximum depth ( $h_{\text{max}}$ ), residual depth ( $h_{\text{res}}$ ), impact velocity  $V_{\text{in}}$  and rebound velocity  $V_{\text{out}}$ . From these the coefficient of restitution ( $e$ ) and % dissipated kinetic energy were determined and changes in these parameters with continued impact were investigated. The coefficient of restitution,  $e$ , is defined as  $|v_{\text{out}}/v_{\text{in}}|$ . The KE loss ratio,  $\lambda$ , is equal to  $1 - e^2$ , and % dissipated energy =  $100 * \lambda$  [22].

An example from a test on AlCrN impacted with a spheroconical probe with 18  $\mu\text{m}$  end radius at 500 mN applied load and 50  $\mu\text{m}$  accelerating distance is shown in figure 2. The contact position ( $h = 0$ ) was defined as the point of maximum velocity ( $V_{\text{in}}$ ). The indenter penetrates the sample to a maximum depth,  $h_{\text{max}}$ .  $V_{\text{out}}$  is the maximum rebound velocity reached before the indenter leaves the surface, at  $h_{\text{res}}$ . The grey region marks the first bounce of the probe.

Scanning electron microscopy (Hitachi Benchtop SEM) in secondary electron (SE) and back-scattered electron mode (BSE SEM) was used to image the impact craters.

### 3. Results

#### 3.1 Nanoindentation

The mechanical properties of the coatings are summarized in Table 3. The AlCrN coating is slightly less hard but stiffer than the TiAlN coating so that the  $H/E$  and  $H^3/E^2$  ratios are higher on the TiAlN.

**Table 3. Coating mechanical properties**

	$H$ (GPa)	$E$ (GPa)	$H/E$	$H^3/E^2$ (GPa)
TiAlN	$37.9 \pm 2.5$	$492.5 \pm 10.5$	0.077	0.224
AlCrN	$36.0 \pm 1.2$	$545.5 \pm 8.8$	0.066	0.158

#### 3.2 Cyclic micro-impact testing

Table 4 summarises the behaviour of the coatings in the cyclic impact tests with the 25  $\mu\text{m}$  probe. Lateral fracture occurred in every test at 2000 and 2500 mN on TiAlN, with a relatively consistent number of impacts ( $\sim 25$ ) required in most tests. This failure was absent in every test on AlCrN at 2000 mN and occurred in 9/15 tests at 2500 mN, although the number of impacts required was more variable than on TiAlN. Typical impact depth vs. number of impacts curves at 2000 and 2500 mN with the  $R = 25 \mu\text{m}$  probe are shown in figure 3(a). The TiAlN coating fails gradually from around 20 impacts at both loads. Although the AlCrN is more resistant to

lateral cracking in cyclic impact, in tests at 2500 mN where it occurred it was more abrupt, e.g. as after 53 impacts in figure 3(a).

**Table 4. Impacts to failure and depth changes in cyclic micro-impact tests with  $R = 25 \mu\text{m}$  probe**

	Load (mN)	Impacts to failure (a)	$h_f - h_1$ ( $\mu\text{m}$ )
TiAlN	2000	$25 \pm 10$	$4.2 \pm 1.0$
	2500	$23 \pm 6$	$5.5 \pm 0.3$
AlCrN	2000	>75	$0.4 \pm 0.0$
	2500	$42 \pm 20$ (b)	$3.4 \pm 2.6$ (c)

(a) Failure defined as the onset of lateral fracture. (b) Failure occurred in 9/15 tests. (c) When failure occurred the mean depth change was  $5.3 \pm 1.3 \mu\text{m}$ ; when failure did not occur it was  $0.5 \pm 0.1 \mu\text{m}$ .

Illustrative SEM images of impact craters are shown in figure 3(b-f). Figure 3(b) shows four impact craters on AlCrN after 75 impacts at 2500 mN, with lateral fracture occurring in two of these. Microscopy showed dramatic lateral fracture in every test with the abrupt increase in depth during the test. In tests where lateral fracture did not occur BSE imaging reveals nested cracks within the crater and radial cracking (fig. 3(c) 2500 mN; fig. 3(d) at 2000 mN). Figure 3(e,f) shows lateral cracking on TiAlN at 2000 and 2500 mN respectively.

Illustrative impact depth vs. number of impacts curves in cyclic tests with the  $R = 18 \mu\text{m}$  probe at 250-1500 mN are shown in figure 4(a,b). **The TiAlN is significantly less impact resistant with lateral fracture occurring at lower load than AlCrN, and fewer impacts being required in**

the tests at higher load. The corresponding depth changes in the test after the initial impact, i.e.  $(h - h_1)$ , for these tests are shown in figure 4(c,d). Figure 4(e,f) shows typical curves on each coating at 750 mN. Both coatings show multi-stage failures. As with the blunter probe, the failure is more gradual on TiAlN and abrupt on AlCrN. There is sharper peak in dissipated energy on AlCrN. In the three 500-impact tests on AlCrN there was some variability, with no failure in one test, one failure in 283 and 457 impacts in the others. The variability was smaller on the TiAlN, requiring 22, 27 and 45 impacts to fail in the three repeat tests at 750 mN. The load dependence of the depth changes in the test ( $h_{\text{final}} - h_1$ ) and the number of impacts required for coating failure are shown in figure 4(g,h).

### 3.3 Statistically distributed micro-impact tests

To assess the influence of applied load independently of distribution the same statistical distribution of impacts was used in the tests at 500-2000 mN with the  $R = 25 \mu\text{m}$  probe. SEM images of the impacted surfaces are shown in figure 5. The extent of chipping and substrate exposure was dependent on the applied load on both coatings. At 500 mN both coatings were resistant to chipping (fig. 5(a,b)). The majority of impacts at this load did not result in any cracking, although BSE imaging revealed some very fine cracks at the intersection of multiple impacts (fig. 5(c,d)). TiAlN was also resistant to chipping at 1000 mN (fig. 5(e)) although more pronounced cracking was observed in multiple impact locations (fig. 5(g)). At this load there was appreciable chipping and substrate exposure on AlCrN (fig. 5(f)). By overlaying the impact locations onto the micrographs it can be seen that the chipped regions and total coating removal and substrate exposure extend well away from the impact sites. The test on AlCrN was repeated with the same result. At 1500 mN and 2000 mN there was chipping and coating removal on both coatings, with the proportion of exposed substrate being significantly higher on AlCrN.

The proportion of chipped area with and without substrate exposure determined from microscopic images of the worn surfaces is shown in fig. 9(a).

Tests were performed at 2500 and 3000 mN with Gaussian and rectangular distributions. SEM images of these are shown in figure 6 and 7. The same pattern of chipping was also seen in tests at 2500 mN with different impact Gaussian distributions. The % chipping and delamination was typically larger on AlCrN (Table 5). At 3000 mN there was also significant chipping and coating removal with the rectangular distribution.

**Table 5. Depth changes in higher load distributed impact tests**

Coating	Load and distribution	Depth increase ( $\mu\text{m}$ )*	% chipped	% chipped
			area without substrate exposure	area with substrate exposure
TiAlN	2500 mN Gaussian	4.57, 5.10	14, 11	19, 16
AlCrN	2500 mN Gaussian	7.28, 8.15	25, 9	27, 21
	2500 mN Rectangular	4.73	21	26
	3000 mN Gaussian	8.41	15	43
	3000 mN Rectangular	4.89	33	43

\* ( $h_{\text{max}} - h_{\text{initial impact}}$ )

Statistically distributed tests with the  $R = 18 \mu\text{m}$  probe showed similar load-dependent behaviour as with the  $25 \mu\text{m}$  probe. From 500 mN there was load-dependent chipping on both

coatings, with the % chipped area (i) increasing with load (ii) being significantly larger on AlCrN (figure 9(b)).

## 4. Discussion

### 4.1 Cyclic micro-impact tests

In the cyclic micro-impact tests with the  $R = 18$  and  $25 \mu\text{m}$  probes the coatings show similar behaviour with failure (lateral fracture) on TiAlN occurring from lower load and being more gradual whereas AlCrN being more resistant to lateral fracture but in tests where it did occur it was quite abrupt, being over in a few impact cycles. Failure occurred at lower load with the sharper probe. In addition to probe sharpness, the tests with the  $18 \mu\text{m}$  probe were more severe as the accelerating distance was greater, resulting in higher impact energies for the same applied load.

With both coatings there is initial (predominantly substrate [23]) plasticity which decreases within a few cycles to a constant (plateau) depth that is followed by a fatigue period where the depth does not increase with continued impact, i.e. there is low cycle fatigue rather than failure due to “ratchetting plasticity” where the coating fails immediately upon reaching a critical bending. With both probes the increase in depth before the start of lateral fracture ( $h_{\text{at failure}} - h_1$ ) was typically around 300-600 nm for both coatings (e.g. as shown in fig. 4(c,d) for the  $R = 18 \mu\text{m}$  probe). In tests on monolayered TiAlCrN, AlTiN and nano-multilayered TiAlCrN/NbN coatings which also undergo lateral fracture, the depth increases before the lateral fracture were similar [13,23]. Although TiAlN and AlCrN both undergo lateral fracture, there may be some differences in mechanism between since on TiAlN the failure was consistently less abrupt and showed a tighter variation in the number of impacts required. Both coatings show multi-stage failures. After the coating lateral fracture and coating damage/removal within the impact crater

there is an initial period of lower damage before the substrate is progressively weakened. Tests have shown that the WC-Co substrate is more resistant to micro-scale impact damage than PVD coatings [13].

Nano-impact tests have been shown to correlate with cutting tests with coatings that display higher resistance to fracture in the nano-impact test exhibiting longer tool life [9-13,17,19]. In cyclic nano-impact tests with much sharper cube corner indenters (15 mN, accelerating distance 12  $\mu\text{m}$ , nominal end radii 50-100 nm) the same clear difference in impact resistance has been previously reported for AlCrN and TiAlN coating samples deposited under the same conditions [17,19]. Failure on AlCrN required more impacts and progressed more gradually, consistent with behaviour in cutting tests such as in high-speed milling of AISI 1045 [18] and 1040 steels [17,19]. For high-speed metal cutting several studies have shown that an optimum - rather than extremely high - coating  $H^3/E^2$  combining load support with crack resistance to be beneficial in extending tool life [24].

In micro-scratch tests with  $R = 25 \mu\text{m}$  probe TiAlN has been reported to fail at lower load ( $4.2 \pm 0.5 \text{ N}$ ) than AlCrN ( $5.7 \pm 0.2 \text{ N}$ ) but the failure was more gradual and localised with a smaller chipped area than observed for AlCrN [17], i.e. with the nominally the same probe geometry and matching contact size there are very similar differences in coating behaviour. A similar correlation between coating behaviour in both tests has also been noted in micro-impact and micro-scratch tests on monolayered  $\text{Al}_{0.67}\text{Ti}_{0.33}\text{N}$ ,  $\text{Ti}_{0.1}\text{Al}_{0.7}\text{Cr}_{0.2}\text{N}$  and  $\text{Ti}_{0.25}\text{Al}_{0.65}\text{Cr}_{0.2}\text{N}$  coatings on cemented carbide [23]. The best performing coating had slightly higher  $H^3/E^2$  and was slightly thicker whilst the poorest performing coating was the thinnest. Daniel and co-workers have performed dynamic macro-scale impact tests on a range of AlCrN coatings [25]. When coating mechanical properties were similar they found enhanced impact resistance for thicker coatings. The slightly lower thickness of the TiAlN may have contributed to its lower impact resistance.

In the tests with the 18  $\mu\text{m}$  probe the energy dissipation was calculated for every impact. This showed that initially there was no difference in energy dissipation between the coatings. Both coatings showed higher dissipated energy at higher load and there was a reduction during first few impact cycles as the contribution from plastic deformation decreased (plasticity exhaustion [22]). However, there were clear and consistent differences in the energy dissipation signature at failure between the coatings (e.g. as shown in fig. 4(e,f)), which was “higher and sharper” for AlCrN and “broader and lower” on TiAlN. Several factors may influence the differences in impact resistance and energy dissipation on failure. The calo-wear tests performed to obtain a smooth surface for nanoindentation unexpectedly revealed a thin ( $\sim 200$  nm) interlayer on the TiAlN which may have helped mitigate against the more abrupt failures that occurred in the AlCrN coating, **where there was no interlayer**. Nanoindentation mapping across the interface revealed the layer had mechanical properties close to that of the cemented carbide substrate. Although the mechanical properties of the two coatings were in a similar range ( $H \sim 36\text{-}38$  GPa,  $E \sim 490\text{-}550$  GPa), there were small differences in  $H/E$  and  $H^3/E^2$ , **which were higher for TiAlN**. It has been observed that coatings with quite high  $H/E$  such as TiAlN can perform poorly in cyclic nano-impact unless there is some compensating microstructural feature, such as having a very dense microstructure [13,17,19].

#### *4.2 Statistically distributed micro-impact*

By programming the same spatial distribution of impacts on both samples in the tests with the 25  $\mu\text{m}$  probe at 500, 1000, 1500 and 2000 mN the load dependence can be clearly shown. As there was a clear transition to chipping and substrate exposure at 1000 mN on AlCrN this test was repeated, e.g. to confirm that it was not an anomalous result from testing in a region with higher coating defects. The chipped area results in the two tests were almost identical (6%

chipped and 12% substrate exposure in one test and 7% chipped and 9% substrate exposure in the other). The tests with the 18  $\mu\text{m}$  probe similarly show a marked change in chipped area with load although the chipping starts at lower load as the probe is sharper and the accelerating distance is greater, and potentially also because the region size was smaller, which increase the overlap.

When the programmed impact locations are overlayed onto the micrographs as in figures 5 and 6 it can be seen that the chipped regions and total coating removal and substrate exposure often extend well away from the individual impact sites. The erosion mechanism involves chipping, aiding removal of material away from initial impact sites. Differences in the morphology of the wear debris, with smaller fragments and very localised cracking on TiAlN may also contribute to the observed differences in erosion rate between the two coatings since the localised fracture reduces the stored energy for significant abrupt lateral fracturing. Interestingly, the crack paths in the low load tests (e.g. 500 and 1000 mN) were straighter on TiAlN (figs. 5c and 5g) and more tortuous on AlCrN (figure 5(d)).

Two alternative approaches for assessing the damage progression cycle-by-cycle with continuing impacts are possible: (1) where the maximum or residual depth is tracked relative to the initial surface (2) where the maximum or residual depth is tracked where the surface is actively defined for every impact. The latter approach has the potential benefit of being able to highlight changes in surface hardening whilst the former more directly correlates with fracture and wear. Figure 7 shows an example where the residual depth relative to the initial surface vs. number of impacts is shown for Gaussian and rectangular distributions on AlCrN at 3000 mN. With the Gaussian distribution fewer impacts were required before the probe depth starts to increase and the resultant depths towards the end of the test are larger. **The maximum depth change during the test can provide an indication of the extent of deformation in tests under different conditions.** Figure 8 shows the load dependence in the maximum depth change in

Gaussian tests to 2000 mN. The depth change can exceed the coating thickness indicating significant substrate plasticity in addition to coating removal. To quantitatively rank performance at the end of the test, the proportion of chipped area with and without substrate exposure can be determined from microscopic images of the worn surfaces (figure 9 and Table 5).

It is clear from the SEM images in figures 5 and 7 and the depth change and chipped area data in figures 8 and 9 and Table 5 that in contrast to the cyclic tests, the TiAlN coating performed significantly better than AlCrN in the distributed micro-impact tests. It is of interest to investigate the influence of coating mechanical properties on this difference. Studies have shown that there is a link between PVD coating mechanical properties such as  $H/E$  and  $H^3/E^2$  and erosion rate, e.g. when eroded by alumina or SiC particles [1,3,26,27]. For example, Yamamoto and co-workers reported the best erosion resistance in TiAlN PVD coatings designed for erosion protection of compressors was for  $H/E \sim 0.07$ , which was also the highest  $H^3/E^2$  of the single-phase cubic TiAlN coatings [3]. Although further increases in Al also produced coatings with high  $H/E$  and  $H^3/E^2$  but these were hexagonal with lower hardness than the alumina erodent leading to higher erosion.

The nanoindentation results in Table 3 show that the TiAlN coating is slightly harder and slightly lower in elastic modulus than the AlCrN which results in a higher  $H/E$  and  $H^3/E^2$  than the AlCrN coating. Although the nanoindentation tests to 30 mN have a small contribution from the substrate (i) there is little elastic mismatch as both coatings are almost as stiff as the cemented carbide (ii) the substrate influence on the measured elasticity will be slightly larger for the thinner TiAlN, so the observed differences between the coatings in terms of  $H/E$  and  $H^3/E^2$  are not an artifact of the small difference in actual coating thickness. It has been suggested that with suitable coating design excellent resistance to solid particle erosion may be achieved with very high  $H^3/E^2$  coatings [1,26,27]. Deng and co-workers reported a relationship

between increasing coating  $H^3/E^2$  and lowering the erosion rate of CrN, TiN, (Cr,Al)N and TiAlN coatings deposited by cathodic arc on cemented carbide when eroded by SiC [26]. The TiAlN coating with higher  $H^3/E^2$  than the (Cr,Al)N (no details of Al:Cr ratio were provided) showed the lowest erosion rate. This behaviour is consistent with the differences in mechanical properties and behaviour observed in the statistically distributed impact test in the current study, where the TiAlN coating with higher  $H^3/E^2$  than the AlCrN performs better.

In future it would be of interest to study the behaviour of a wider range of hard PVD coatings in the statistically distributed impact test since it appears that coating design to solely to maximise  $H^3/E^2$ , to effectively limit crack initiation, may not always help with the lateral crack propagation. The latter can result in higher erosion rates and some studies [29,30] have reported poor erosion resistance for coatings with extremely high  $H^3/E^2$ . The highest resistance to erosion by alumina was reported for 6  $\mu\text{m}$  TiAlN coatings on Ti6Al4V that had intermediate  $H^3/E^2$  amongst the coatings tested [29]. Similarly, Krella [30] has noted that several studies have shown the best resistance to solid particle erosion and cavitation erosion for coatings with  $H/E \sim 0.07$ , with worse performance for coatings with  $H/E > 0.08$ .

#### *4.3 Comparison between coating behaviour in cyclic micro-impact and statistically distributed micro-impact tests*

In these tests there is a connection between whether the impact fracture is abrupt or gradual in the cyclic impact tests and the extent of lateral fracture in the statistically distributed tests. The interaction between radial/lateral cracks generated by repetitive contact is an important mechanism for chipping fracture and coating material removal. The susceptibility of the coating system to lateral vs. localised cracking (and differences in their “interaction thresholds”) controls the rate of damage accumulation and material removal in micro-impact

and in erosion. These differences in cracking type and interaction threshold appear to control the rate of material removal in micro-impact tests on glasses [15] and in the bulk technical ceramics MgO-stabilised zirconia, alumina and sapphire (0001) [31].

Higher load/more impacts were required to cause coating failure in the cyclic test than in the distributed impact test. In tests with  $R = 25 \mu\text{m}$  probe, AlCrN failed at 1000 mN in the distributed test but intermittently at 2500 mN in the cyclic test. In tests with  $R = 18 \mu\text{m}$  probe, after 50 impacts at 1000 mN there was no failure on AlCrN but in the distributed tests there was failure even at 500 mN. Similarly, on TiAlN, there was more failure with less impacts and/or at lower load in the statistical tests than in the cyclic tests. The results indicate that subsequent impacts in the same position are not as effective at causing the lateral chipping as can occur from the interaction of radial cracks emanating from multiple impact sites.

The different types of micro-scale impact test are most effective in simulating different contact conditions. Cyclic impact has found particular application in replicating metal cutting where the repetitive contact occurs at the same position [9-13,17]. Relative changes in coating cutting tool life through, e.g. small compositional or residual stress modifications, have been exactly mirrored in cyclic impact tests [9-11,13]. Coating behaviour in the cyclic test has also been reported to show a correlation to erosion resistance [6-8]. However, the statistically distributed micro-impact test can also replicate the distribution of individual impacts that occur when a surface is subjected to solid particle erosion [15,16]. Future development of the statistically distributed micro-impact test could include even closer simulation through varying angle incidence for impacts, introducing statistical distribution of loads and testing at elevated temperatures to simulate high temperature erosion. To date, cyclic impact tests have been performed on hard PVD coatings to 600 °C [32] and statistically distributed tests up to 850 °C on 7YSZ thermal barrier coatings [33]. Alternative test probe materials, such as WC, could be used to investigate the influence of the relative hardness of probe and sample on the impact

mechanisms which has been shown to influence erosion [34,35]. Statistically distributed and cyclic micro-impact tests are typically accelerated tests that provide a severe environment so that the surface is subjected to high contact stresses (including high bending stresses for coatings, through high loads and small contacts). Since the tests are quick it is feasible to complement them with tests involving higher numbers of impacts at lower stresses to replicate behaviour in less demanding conditions.

## 5. Conclusions

The relative performance of the TiAlN and AlCrN coatings **studied was** dependent on the type of micro-impact test. TiAlN performed significantly better than AlCrN in the statistically distributed micro-impact test but AlCrN performed significantly better than TiAlN in the cyclic micro-impact test. Differences in the coating system susceptibility to localised cracking appear responsible. Localised cracking in TiAlN causes degradation in cyclic impact and relieves the strain accumulation and dramatic chipping that occurs on AlCrN.

**The different types of micro-scale impact test are most effective in simulating different contact conditions. Cyclic impact has proved reliable for replicating metal cutting where the repetitive contact occurs at the same position, although performance in the cyclic test may also closely correlate with erosion resistance. However, the statistically distributed micro-impact test can also replicate the distribution of individual impacts that occur when a surface is subjected to solid particle erosion, and thus may ultimately prove a more useful test for coating screening for erosion resistance.**

## 6. References

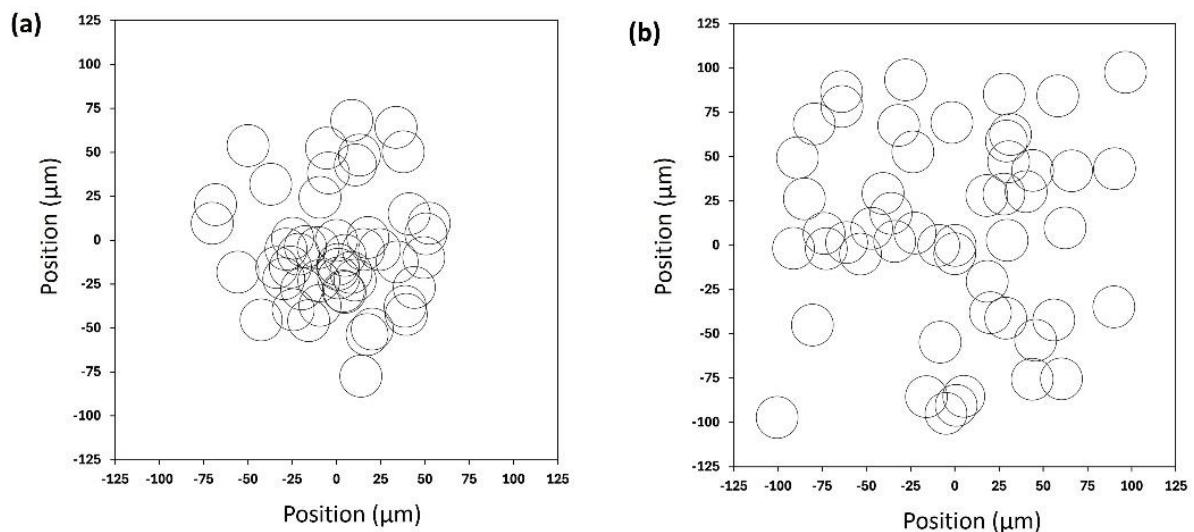
1. E. Bousser, L. Martinu, J.E. Klemberg-Sapieha, Solid particle erosion mechanisms of protective coatings for aerospace applications, *Surf. Coat. Technol.* 257 (2014) 165-181.
2. V. Bonu and H.C. Barshilia, High-temperature solid particle erosion of aerospace components: its mitigation using advanced nanostructured coating technologies, *Coatings* 12 (2022) 1979.
3. K. Yamamoto, Y. Tatsuhira, Y. Iwai, The relationship between coating property and solid particle erosion resistance of AIP-deposited TiAlN coatings with different Al contents, *Coatings* 11 (2021) 992.
4. Y. Ren, Z. Zhang, G. He, Y. Chai, Y. Zhang, Z. Zhang, Erosion performance of TiN/Ti coatings under different nitrogen flow rates, *Coatings* 14 (2024) 1144.
5. Q. Yang, R. McKellar, Nanolayered CrAlTiN and multilayered CrAlTiN-AlTiN coatings for solid particle erosion protection, *Tribol. Int.* 83 (2015) 12-20.
6. J. Chen, B.D. Beake, R.G. Wellman, J.R. Nicholls, H. Dong, An investigation into the correlation between nano-impact resistance and erosion performance of EB-PVD thermal barrier coatings on thermal ageing, *Surf. Coat. Technol.* 206 (2012) 4992-4498.
7. S.J. McMaster, T.W. Liskiewicz, A. Neville, B.D. Beake, Probing fatigue resistance in multi-layer DLC coatings by micro- and nano-impact: Correlation to erosion tests, *Surf. Coat. Technol.* 402 (2020) 126319.
8. L. Ventakesh, S.B. Pitchuka, G. Sivakumar, R.C. Gundakaram, S.V. Joshi, Microstructural response of various chromium carbide based coatings to erosion and nano impact testing, *Wear* 386-387 (2017) 72-79.
9. K.-D. Bouzakis, F. Flocke, G. Skordaris, E. Bouzakis, S. Geradis, G. Katirtzoglou and S. Makrimalakis, Influence of dry micro-blasting grain quality on wear behaviour of TiAlN coated tools, *Wear* 271 (2011) 783-791.
10. G. Skordaris K.-D. Bouzakis, P. Charalampous, E. Bouzakis, R. Paraskevopoulou, O. Lemmer, S. Bolz, Brittleness and fatigue effect of mono- and multi-layer PVD films on the cutting performance of coated cemented carbide inserts, *CIRP Annals - Manuf Tech* 63 (2014) 93.
11. G. Skordaris, K.D. Bouzakis, T. Kotsanis, P. Charalampous, E. Bouzakis, B. Breidenstein, B. Bergmann, B. Denkena, Effect of PVD film's residual stress on their mechanical properties, brittleness, adhesion and cutting performance of coated tools, *CIRP. J. Manufact. Sci. Technol.* 18 (2017) 145-151.
12. B.D. Beake, J.F. Smith, A. Gray, G.S. Fox-Rabinovich, S.C. Veldhuis, J.L. Endrino, Investigating the correlation between nano-impact fracture resistance and hardness/modulus ratio from nanoindentation at 25-500°C and the fracture resistance and lifetime of cutting tools with Ti<sub>1-x</sub>Al<sub>x</sub>N (x=0.5 and 0.67) PVD coatings in milling operations, *Surf. Coat. Technol.* 201 (2007) 4585.
13. B.D. Beake, Nano- and micro-scale impact testing of hard coatings: a review, *Coatings* 12 (2022) 793.
14. UK Patent Application #2217939.4 Surface Testing Apparatus (Erosion) 29/11/22.
15. B.D. Beake, S.R. Goodes, H. Zhang, L. Isern, C. Chalk, J.R. Nicholls, M.G. Gee, Randomised nano-/micro- impact testing – a novel experimental test method to simulate erosive damage caused by solid particle impacts, *Tribol. Int.* 195 (2024) 109647.
16. B.D. Beake, L. Isern, H. Zhang, C. Chalk, S.R. Goodes, D. Johnson, K. Almandoz Forcen, J.R. Nicholls, M.G. Gee, Damage mechanisms in solid particle impact and erosion testing of thermal barrier coatings (in preparation).

17. G.S. Fox-Rabinovich, B.D. Beake, J.L. Endrino, S.C. Veldhuis, R. Parkinson, L.S. Shuster et al. Effect of mechanical properties measured at room and elevated temperatures on the wear resistance of cutting tools with TiAlN and AlCrN coatings. *Surf. Coat. Technol.* 200 (2006) 5738-5742.
18. W. Kalss, A. Reiter, V. Derflinger, C. Gey, J.L. Endrino, Modern coatings in high performance cutting applications. *Int. J. Refract. Metal. Hard Mater.* 24 (2006) 399-404.
19. B.D. Beake, G.S. Fox-Rabinovich, S.C. Veldhuis, S.R. Goodes, Coating optimisation for high-speed machining with advanced nanomechanical test methods. *Surf. Coat. Technol.* 203 (2009) 1919-1925.
20. B.D. Beake, J.L. Endrino, C. Kimpton, G.S. Fox-Rabinovich, S.C. Veldhuis, Elevated temperature repetitive micro-scratch testing of AlCrN, TiAlN and AlTiN PVD coatings. *Int. J. Refract. Metal. Hard Mater.* 69 (2017) 215-226.
21. ISO 14577, parts 1-4, Metallic materials – instrumented indentation test for hardness and materials parameters.
22. F. De Luca, H. Zhang, K.P. Mingard, M. Gee, Nanomechanical response of tungsten carbide single crystals in extreme conditions: temperature and strain rate dependence, *MTLA* 27 (2023) 101706.
23. B.D. Beake, L. Isern, J.L. Endrino, G.S. Fox-Rabinovich, Micro-impact testing of AlTiN and TiAlCrN coatings. *Wear* 418–419 (2019) 102-110.
24. B.D. Beake, G.S. Fox-Rabinovich, Progress in high temperature nanomechanical testing of coatings for optimising their performance in high speed machining, *Surf. Coat. Technol.* 255 (2014) 1021115.
25. J. Daniel, R. Zemlicka, M. Alishahi, P. Karvankova, P. Soucek, D. Karpinski et al, Dynamic impact resistance and scratch adhesion of AlCrN coatings sputtered using cathodic arc glow discharge, *Coatings* 13 (2023) 515.
26. J. Deng, F. Wu, Y. Li, Y. Xing, S. Li, Erosion wear of CrN, TiN, CrAlN and TiAlN PVD nitride coatings, *Int. J. Refract. Met. Hard Mater.* 35 (2012) 10-16.
27. S. Hassani, M. Bielawski, W. Beres, L. Martinu, M. Balazinski and J.E. Klemberg-Sapieha, Predictive tools for the design of erosion resistant coatings, *Surf. Coat. Technol.* 203 (2008) 204-210.
28. Q. Yang, D.Y. Seo, L.R. Zhao, X.T. Zeng, Erosion resistance performance of magnetron sputtering deposited TiAlN coatings, *Surf. Coat. Technol.* 188-189 (2004) 168.
29. B. Borawski, J. Singh, J.A. Todd, D.E. Wolfe, Multi-layer coating design architecture for optimum particulate erosion resistance, *Wear* 271 (2011) 2782-2792.
30. A. Krella, Resistance of PVD coatings to erosive and wear processes: a review, *Coatings* 10 (2020) 921.
31. B.D. Beake, unpublished work.
32. B.D. Beake, A. Bird, L. Isern, J.L. Endrino, F. Jiang, Elevated temperature micro-impact testing of TiAlSiN coatings produced by physical vapour deposition, *Thin Solid Films* 688 (2019) 137358.
33. B.D. Beake, J. Roberts, L. Isern, C. Chalk, J.R. Nicholls, Elevated temperature micro-scale impact testing of thermal barrier coatings for erosion simulation, ICMCTF 2024, San Diego, USA.
34. S. Wada, Effects of Hardness and Fracture Toughness of Target Materials and Impact Particles on Erosion of Ceramic Materials, *Key Eng. Mater.* 71 (1992) 57-74.
35. P.H. Shipway, I.M. Hutchings, The rôle of particle properties in the erosion of brittle materials, *Wear* 193 (1996) 105-113.

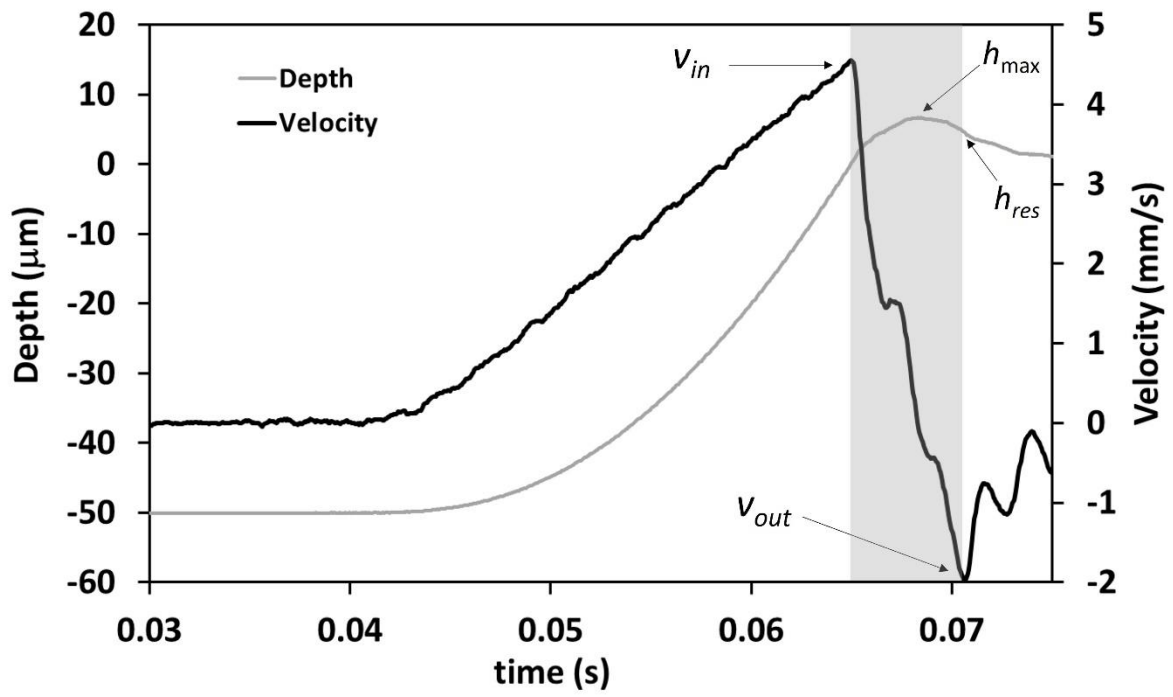
## Figure Captions

1. Typical statistical distributions (a) Gaussian (b) rectangular, within  $200\ \mu\text{m} \times 200\ \mu\text{m}$  regions.
2. Example of a single impact
3. Cyclic impact with  $R = 25\ \mu\text{m}$ . (a) Impact depth data. SEM images. (b) craters on AlCrN at 2500 mN; (c) higher resolution image showing radial cracking; (d) typical impact crater on AlCrN at 2000 mN; (e) typical impact crater on TiAlN at 2000 mN (f) typical impact crater on TiAlN at 2500 mN.
4. Cyclic impact with  $R = 18\ \mu\text{m}$ . Load dependence on (a) TiAlN (b) AlCrN. Depth increases on (c) TiAlN and (d) AlCrN. Variation in impact depth and energy dissipation in typical tests at 750 mN on (e) TiAlN and (f) AlCrN.
5. SEM images from statistically distributed impact tests with  $R = 25\ \mu\text{m}$ ; Gaussian distribution 500-2000 mN. (a) 500 mN on TiAlN (b) 500 mN on AlCrN (c) higher resolution BSE image on TiAlN at 500 mN (d) higher resolution BSE image on AlCrN at 500 mN (e) 1000 mN on TiAlN (f) 1000 mN on AlCrN (g) higher resolution BSE image on TiAlN at 1000 mN (h) 1500 mN on TiAlN (i) 1500 mN on AlCrN (j) higher resolution image on TiAlN at 1500 mN (k) 2000 mN on TiAlN (l) 2000 mN on AlCrN.
6. SEM images from statistically distributed impact tests with  $R = 25\ \mu\text{m}$ ; 2500 and 3000 mN. (a) 2500 mN Gaussian on TiAlN (b) 2500 mN Gaussian on AlCrN (c) BSE image 2500 mN on TiAlN (d) 3000 mN Gaussian on AlCrN (e) 3000 mN rectangular on TiAlN (f) 2500 mN rectangular on AlCrN, with higher resolution BSE image in (g).
7. Dissipated energy and impact depth in distributed impact tests on AlCrN at 3000 mN with (a) Gaussian and (b) rectangular distributions.
8. Load dependence in maximum depth increases in statistically distributed impact tests.
9. Load dependence in chipped area with and without substrate exposure for (a)  $R = 25\ \mu\text{m}$  and (b)  $R = 18\ \mu\text{m}$  probes.

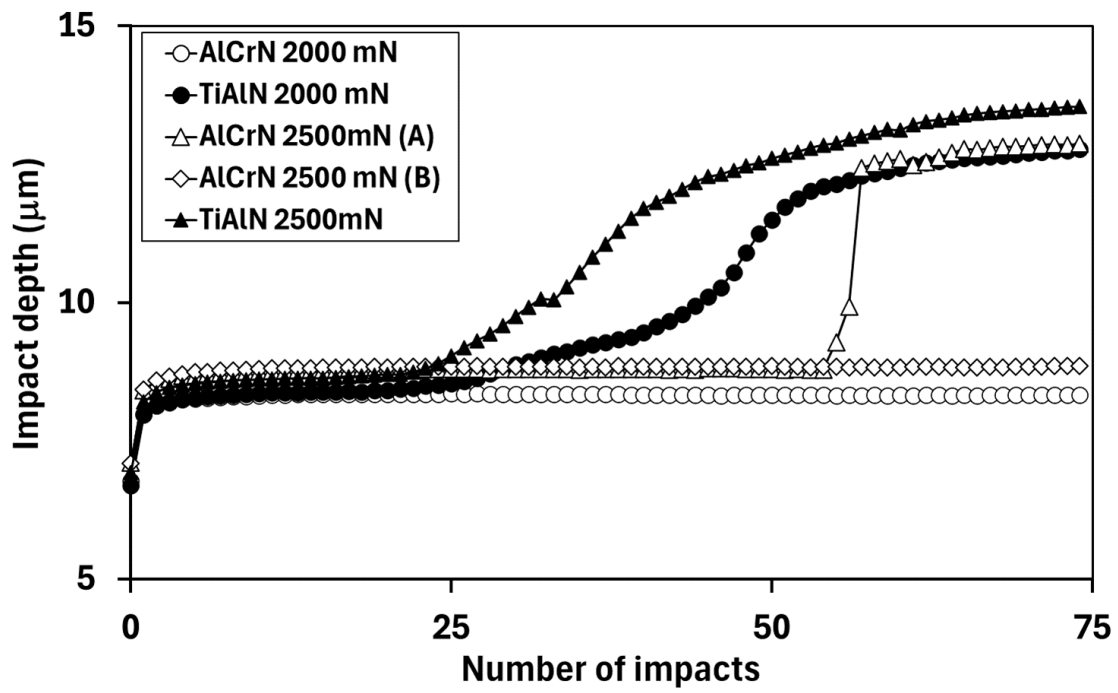
## Figures



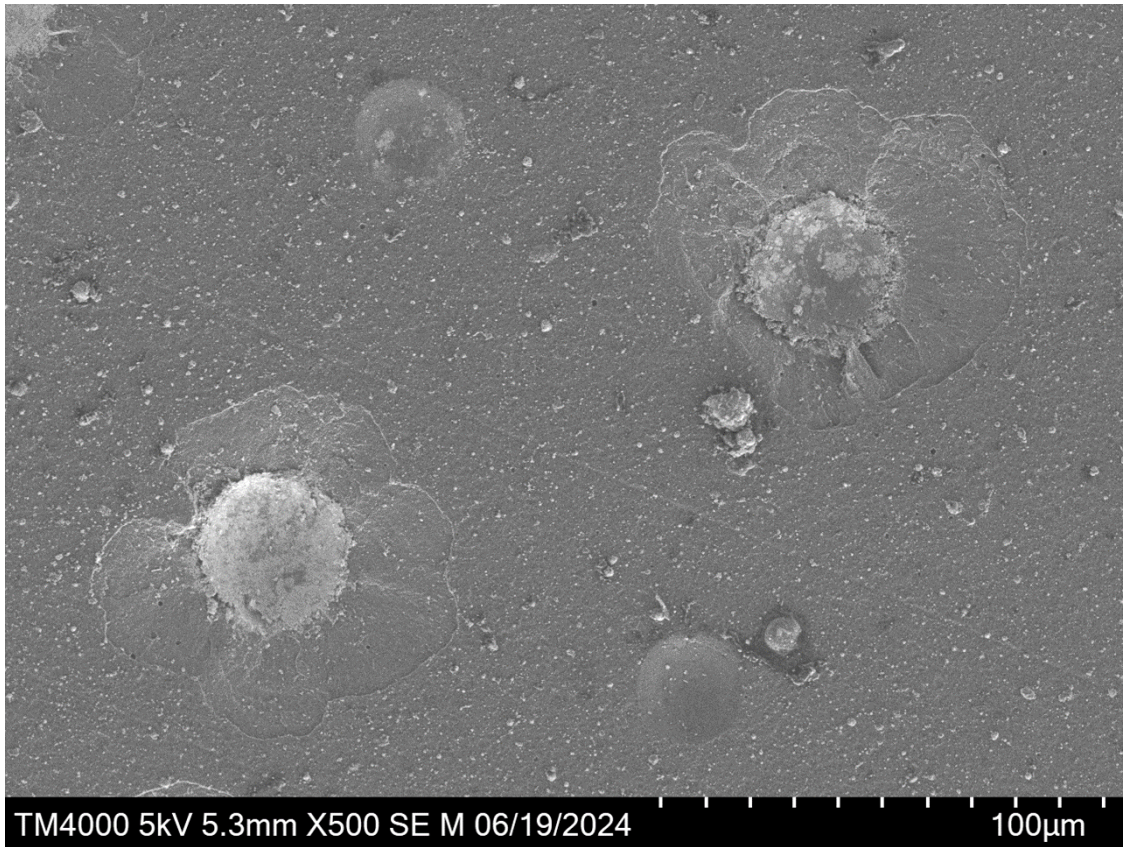
1.



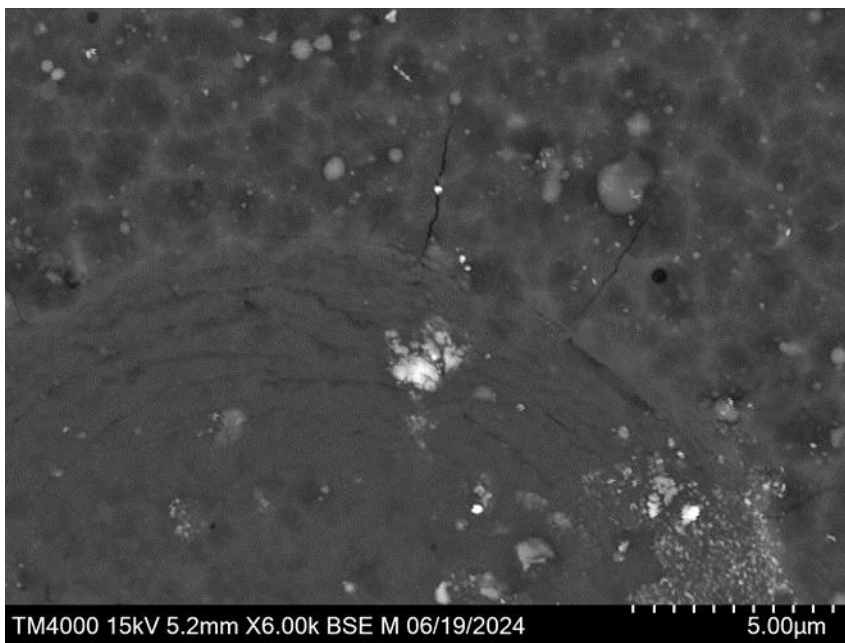
2.



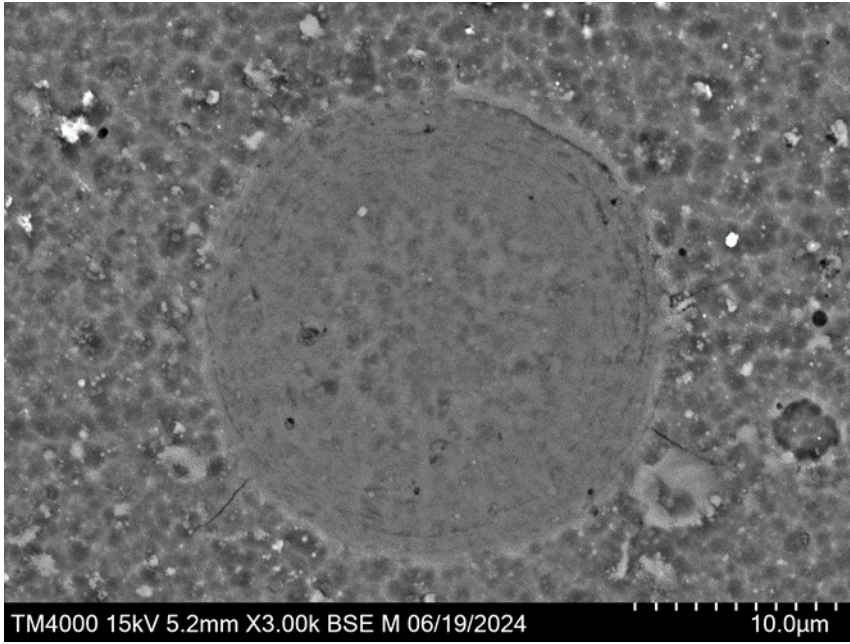
3(a)



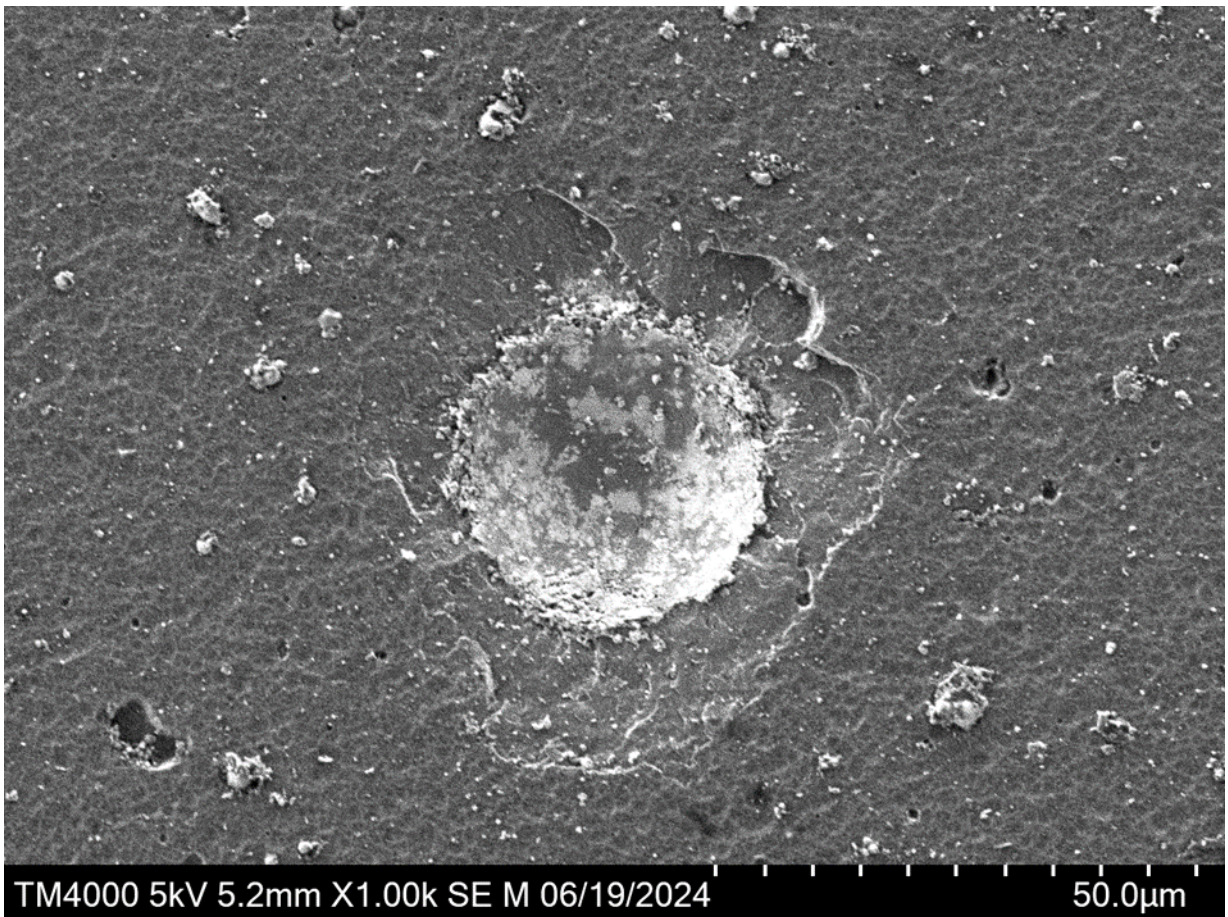
3(b)



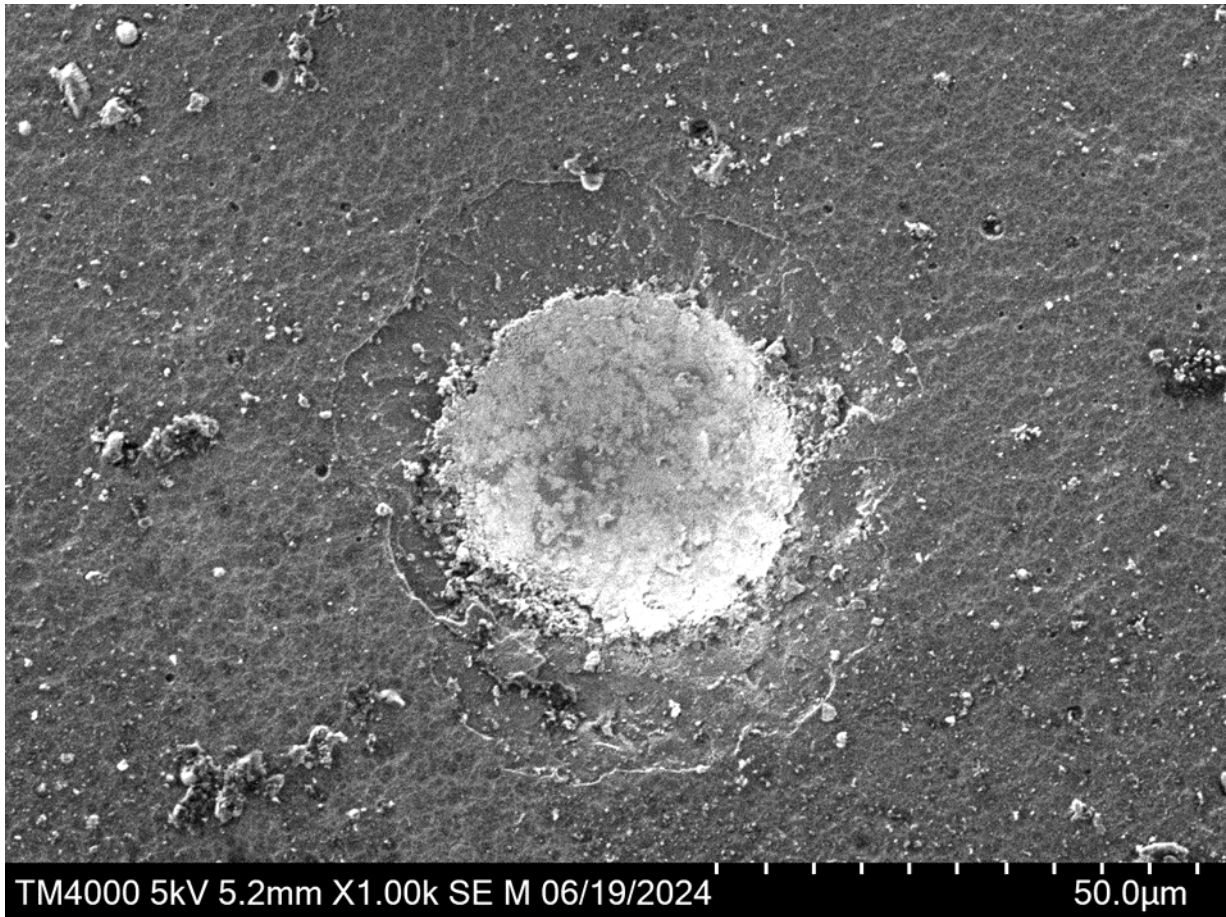
3(c)



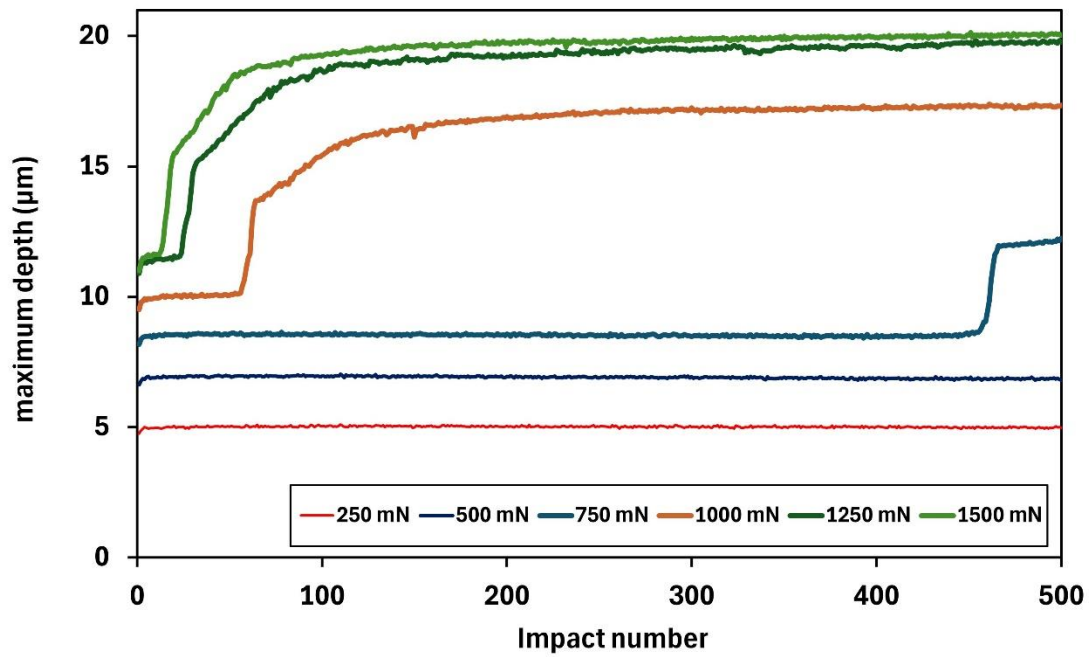
3(d)



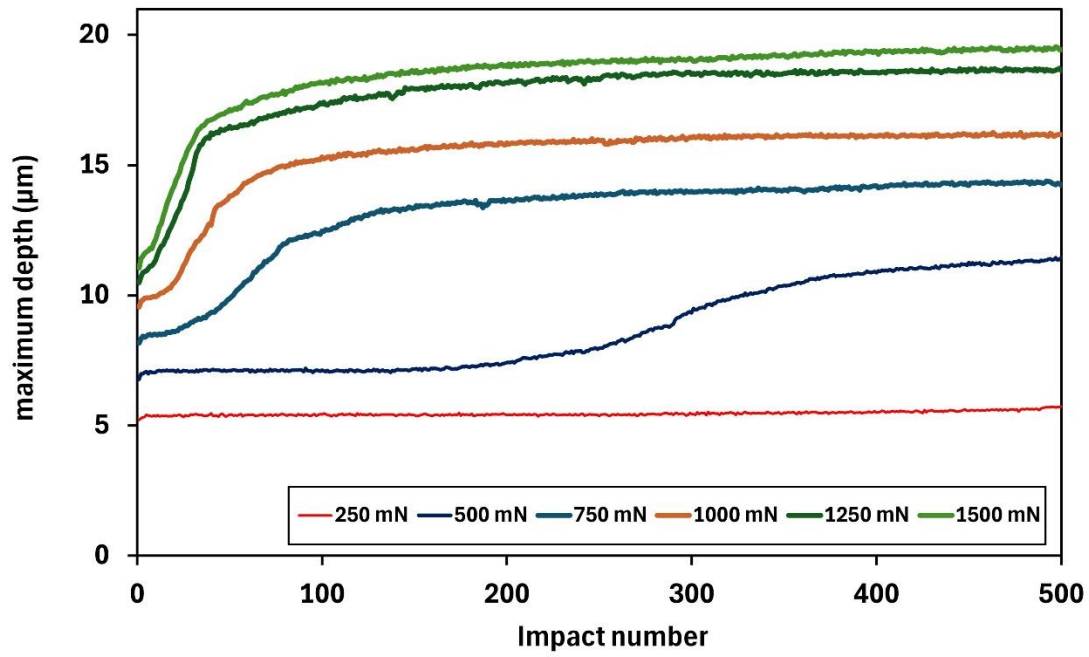
3(e)



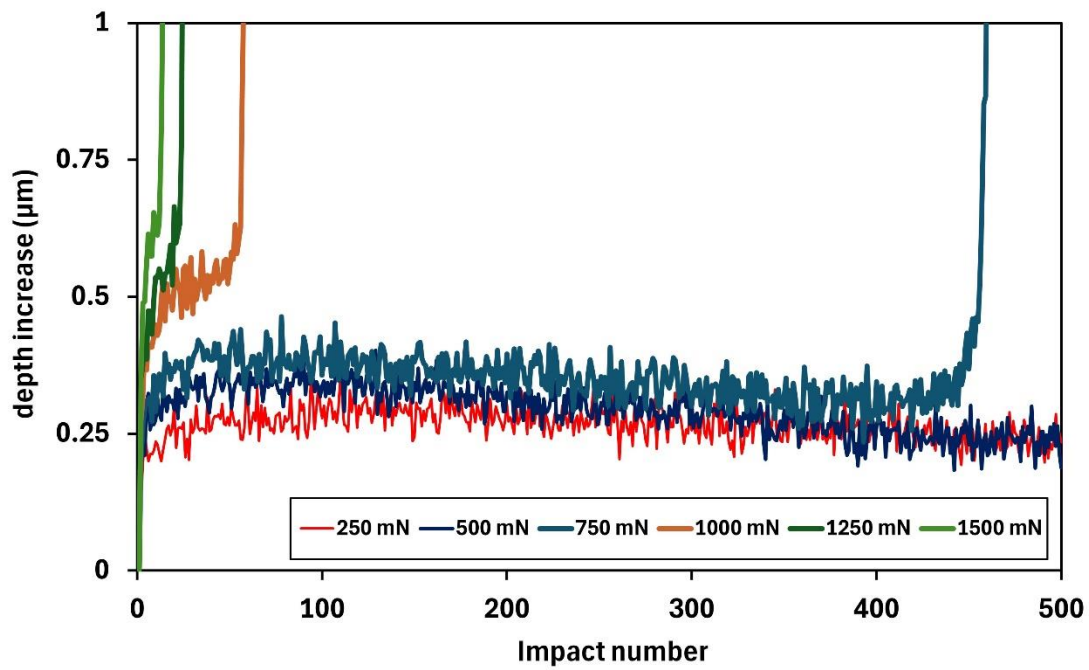
3(f)



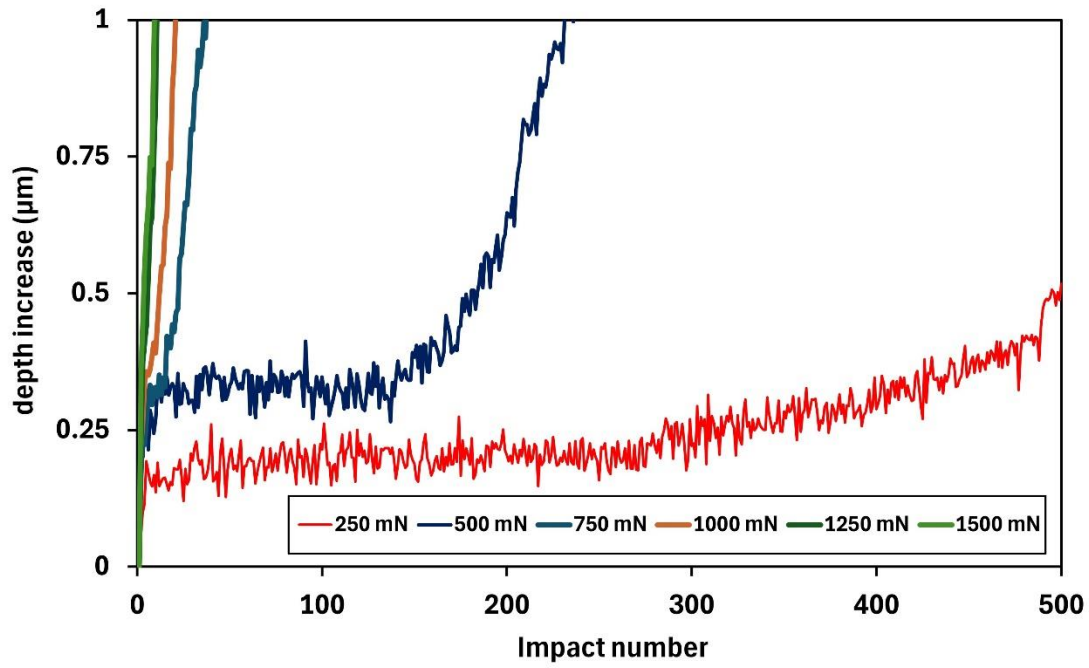
4(a)



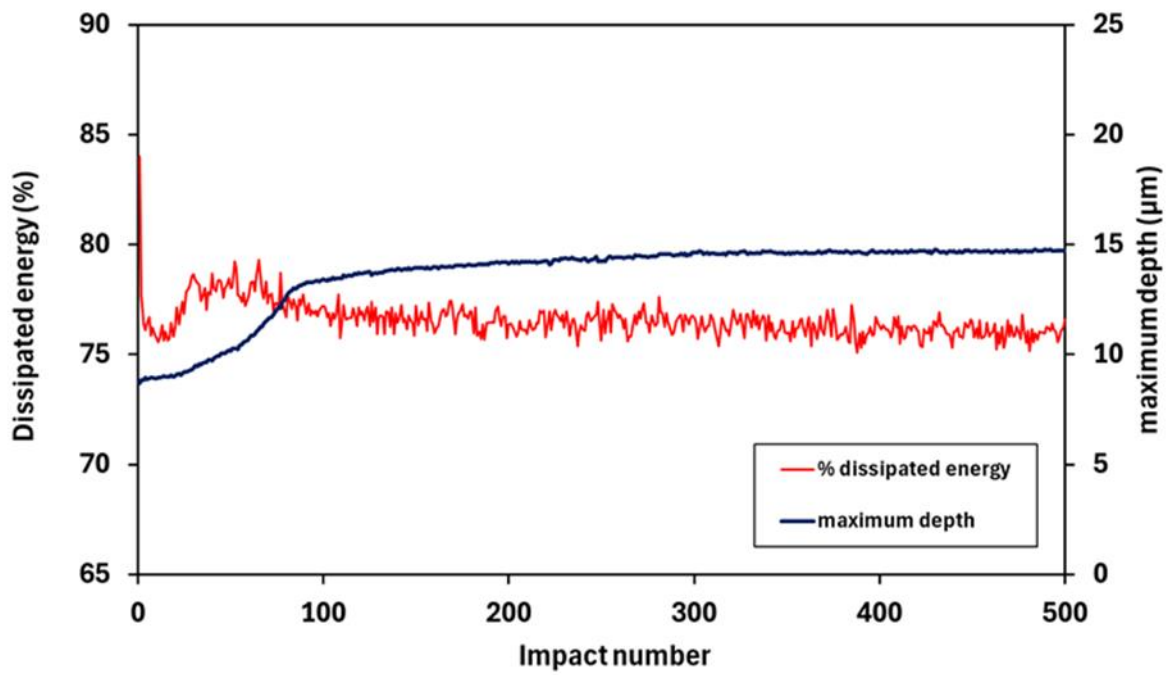
4(b)



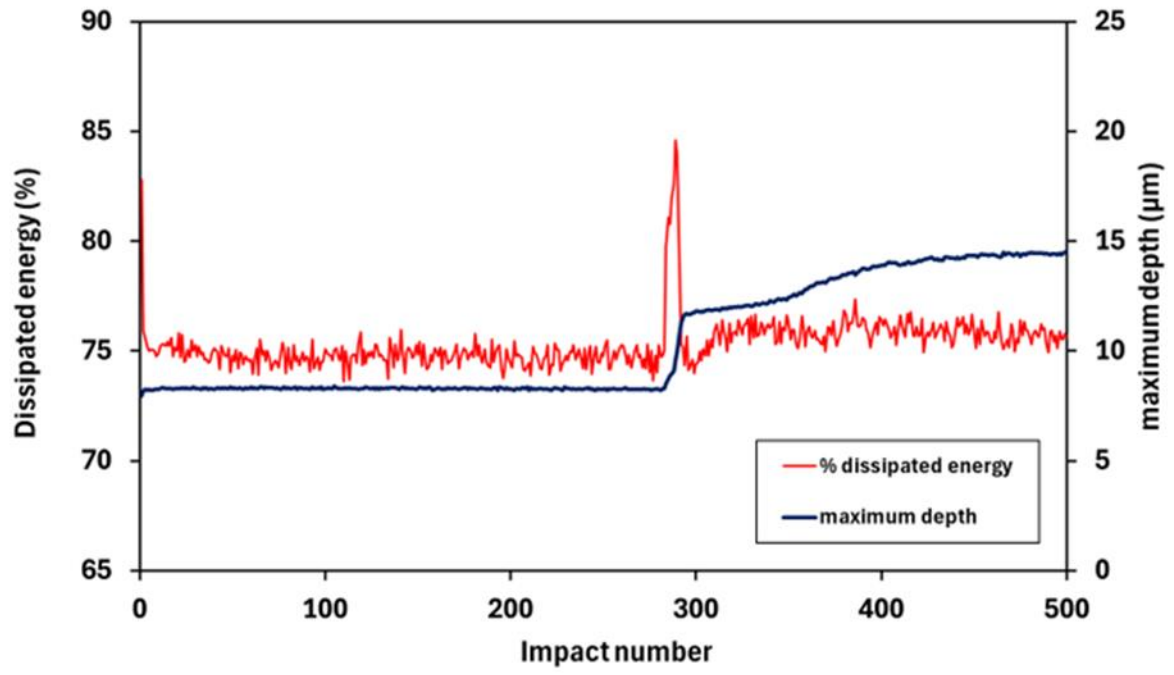
4(c)



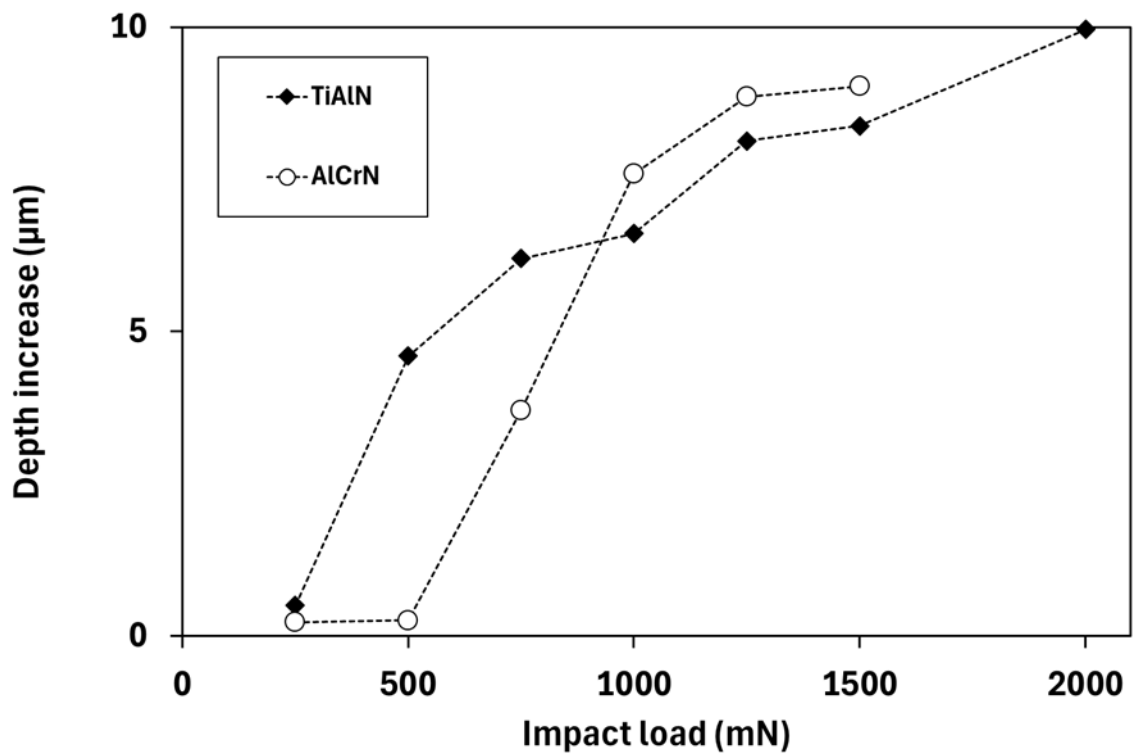
4(d)



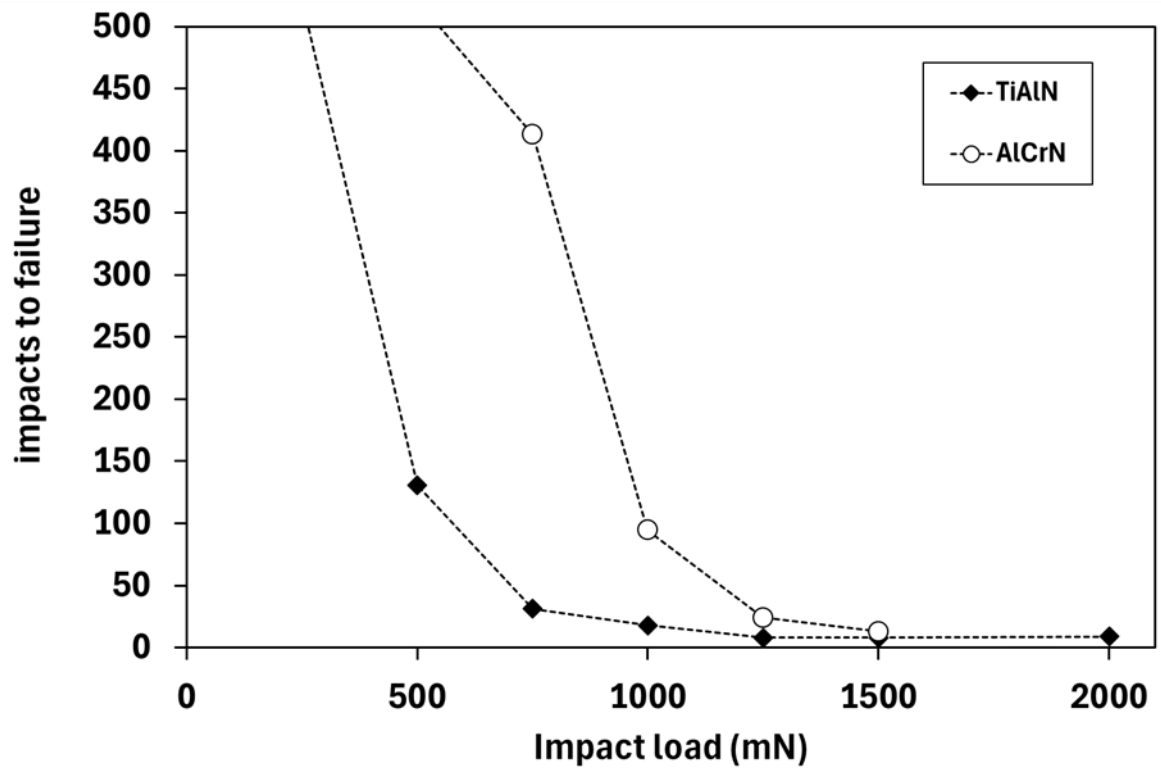
4(e)



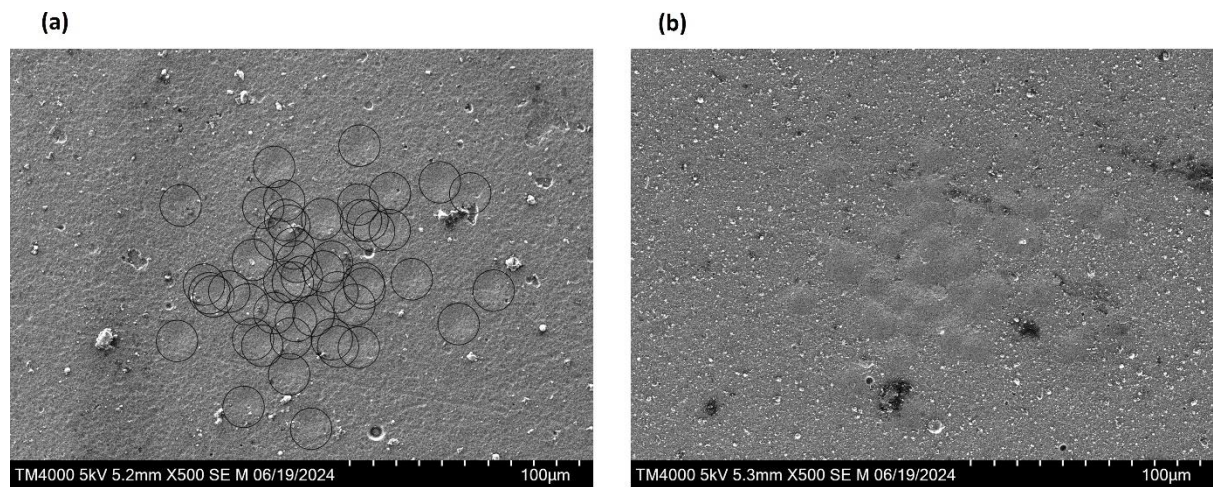
4(f)



4(g)

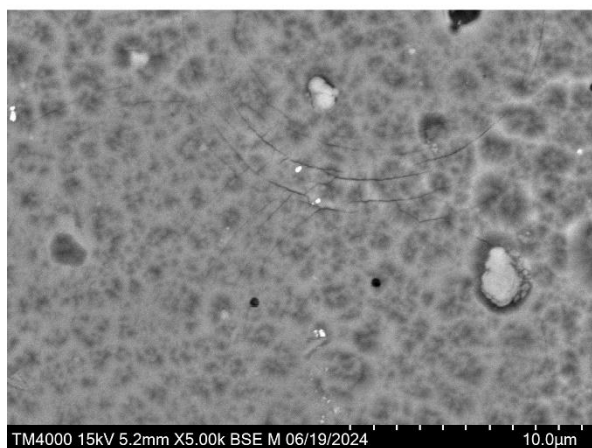


4(h)

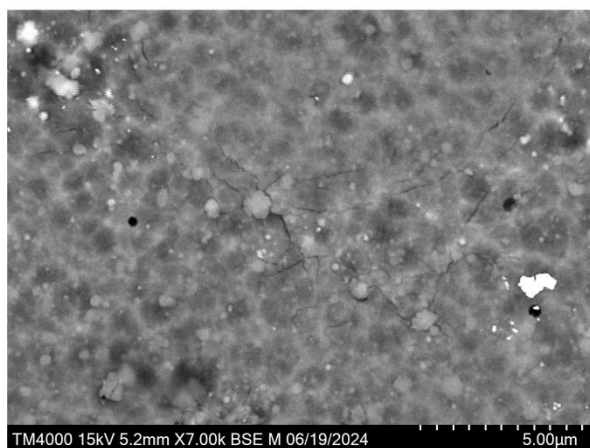


5(a,b)

(c)

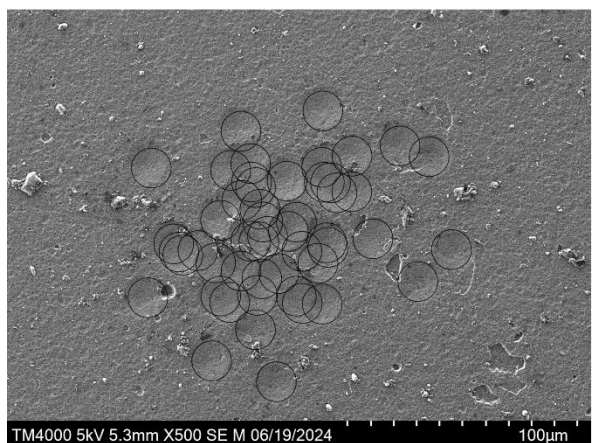


(d)

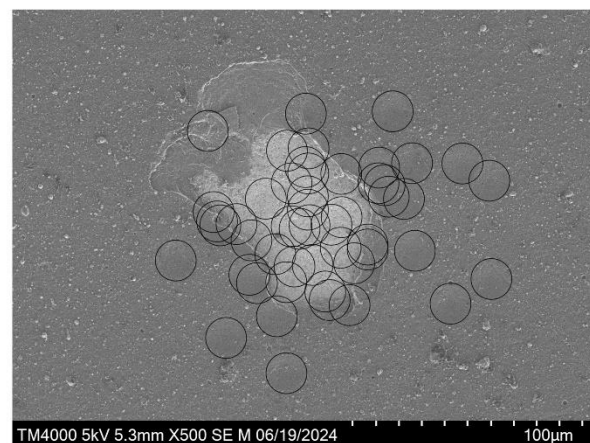


5(c,d)

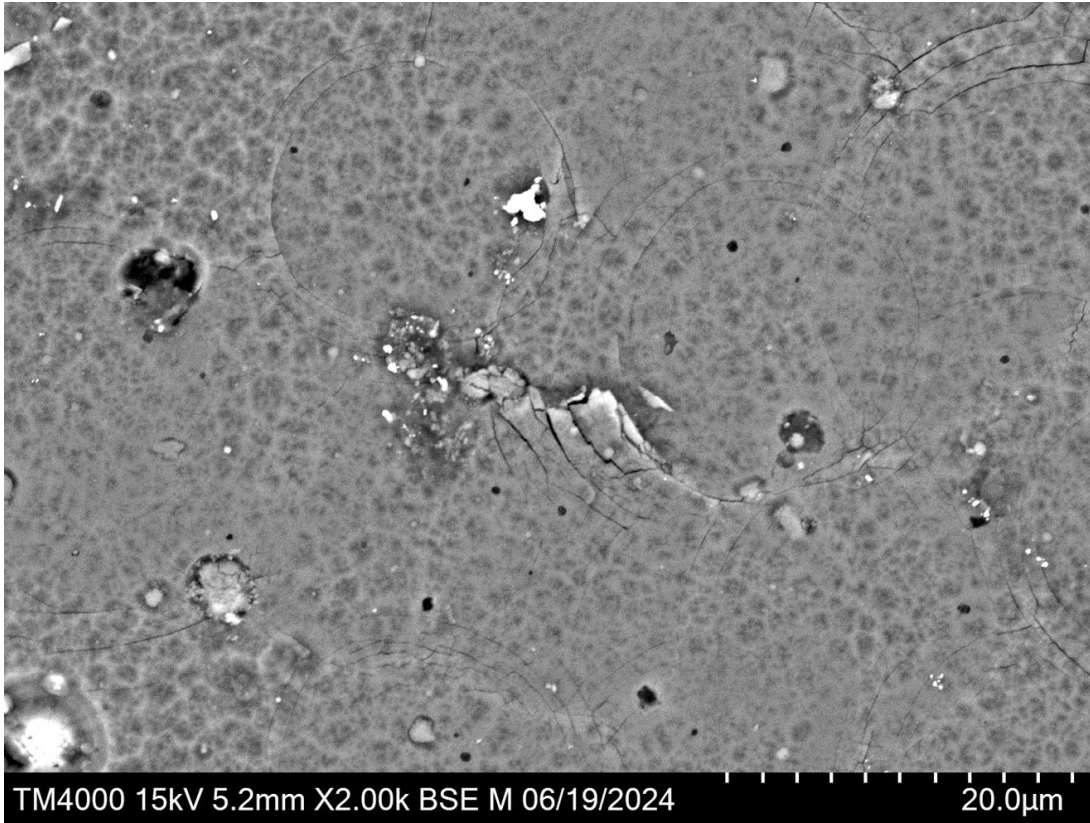
(e)



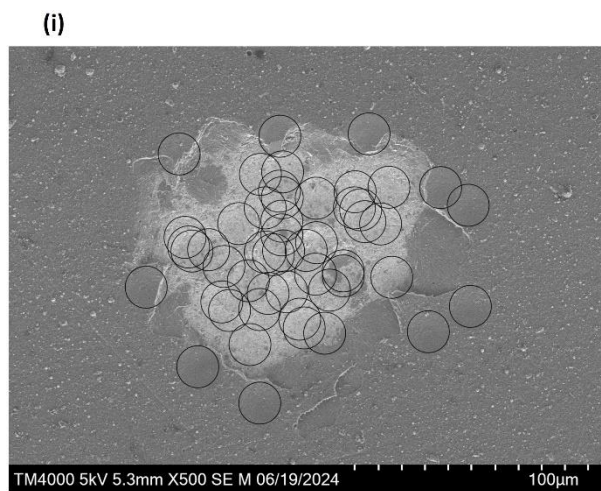
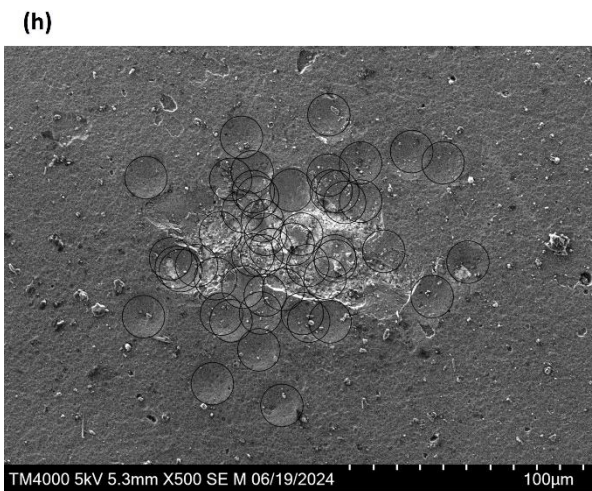
(f)



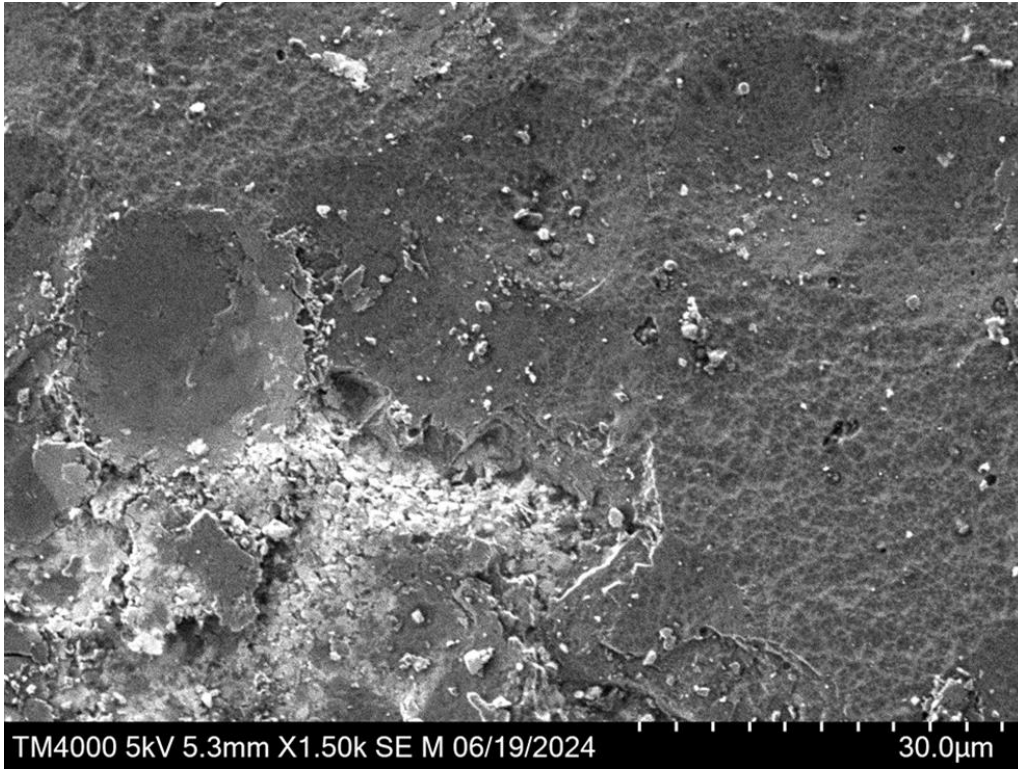
5(e,f)



5(g)

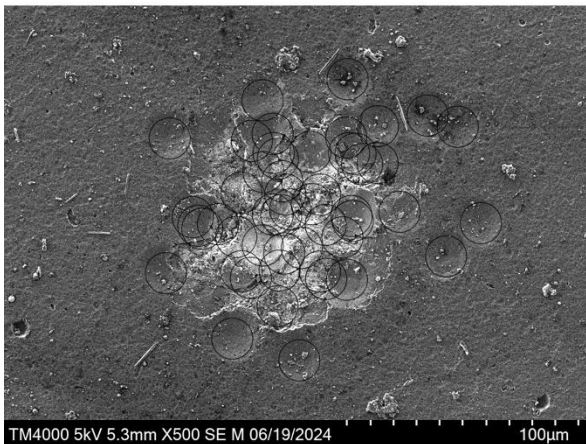


5(h,i)

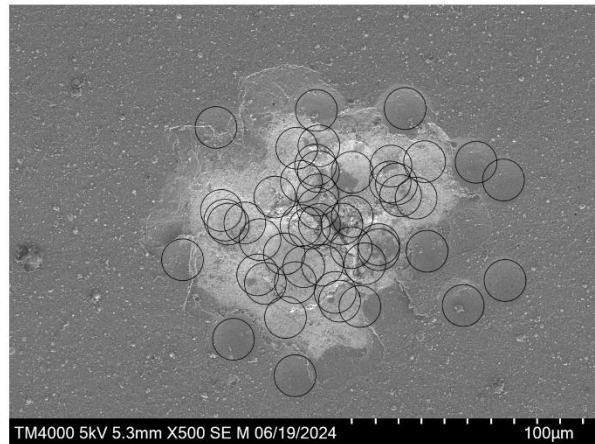


5(j)

(k)

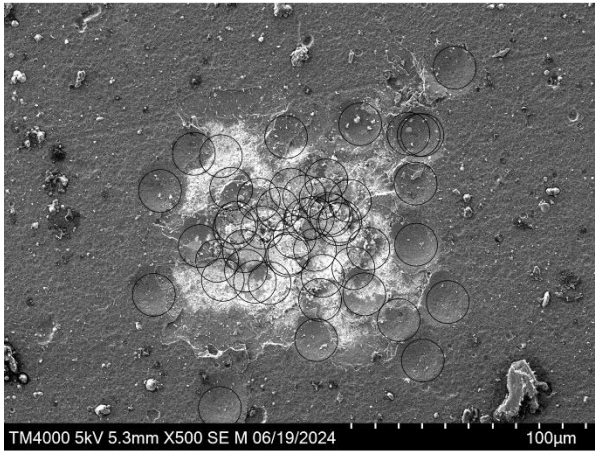


(l)

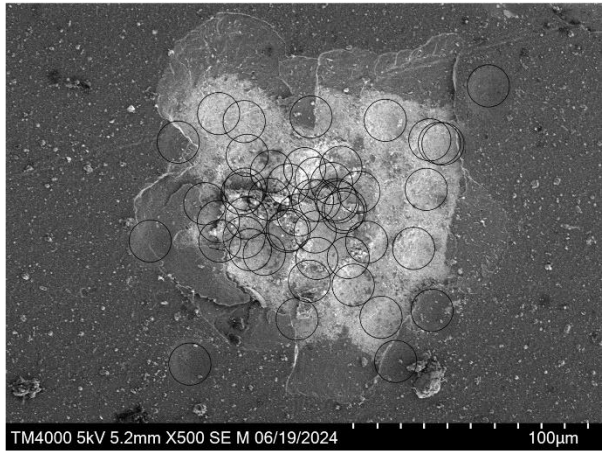


5(k,l)

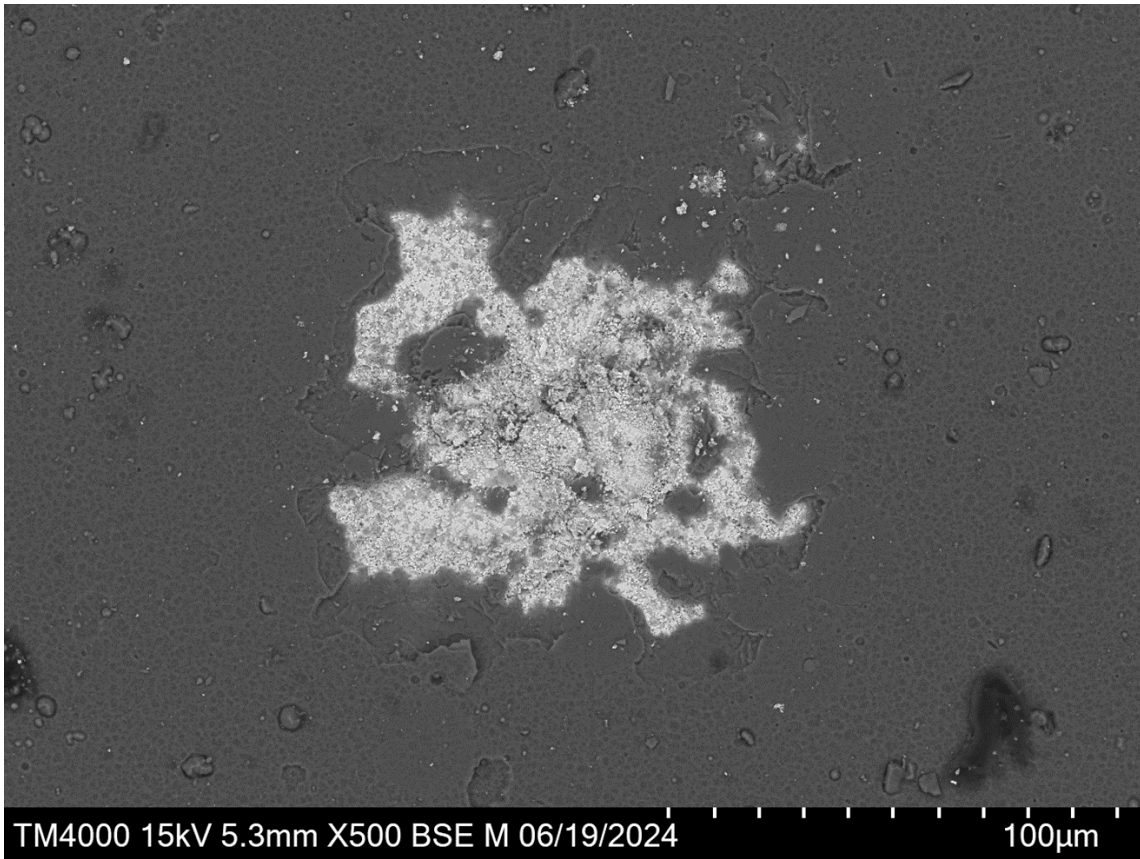
(a)



(b)

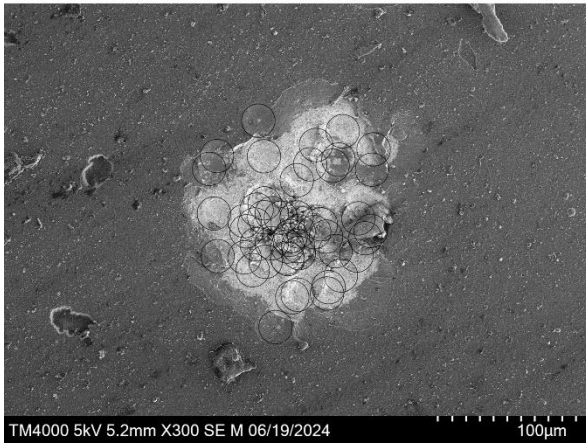


6(a,b)

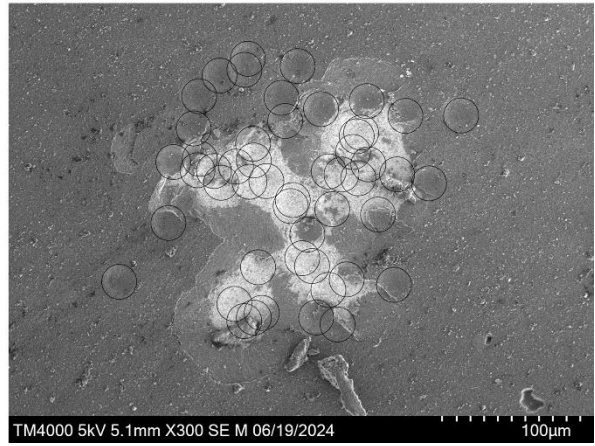


6(c)

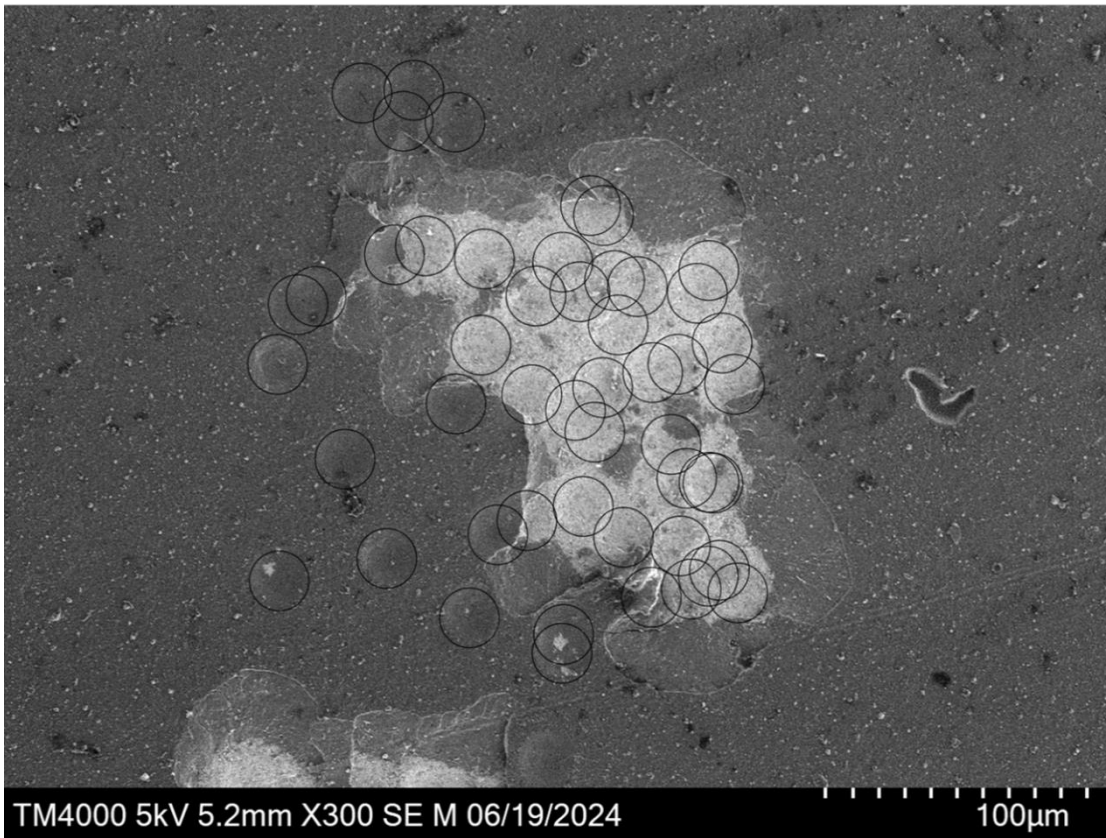
(d)



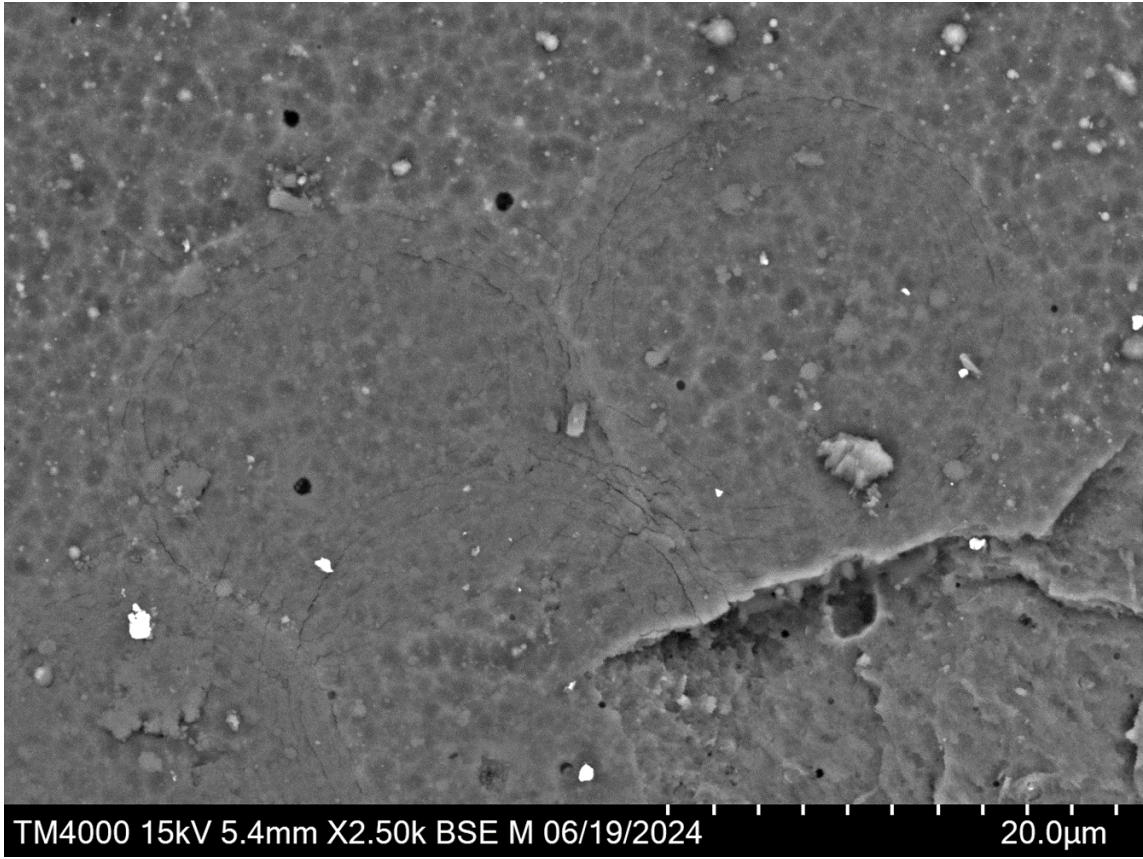
(e)



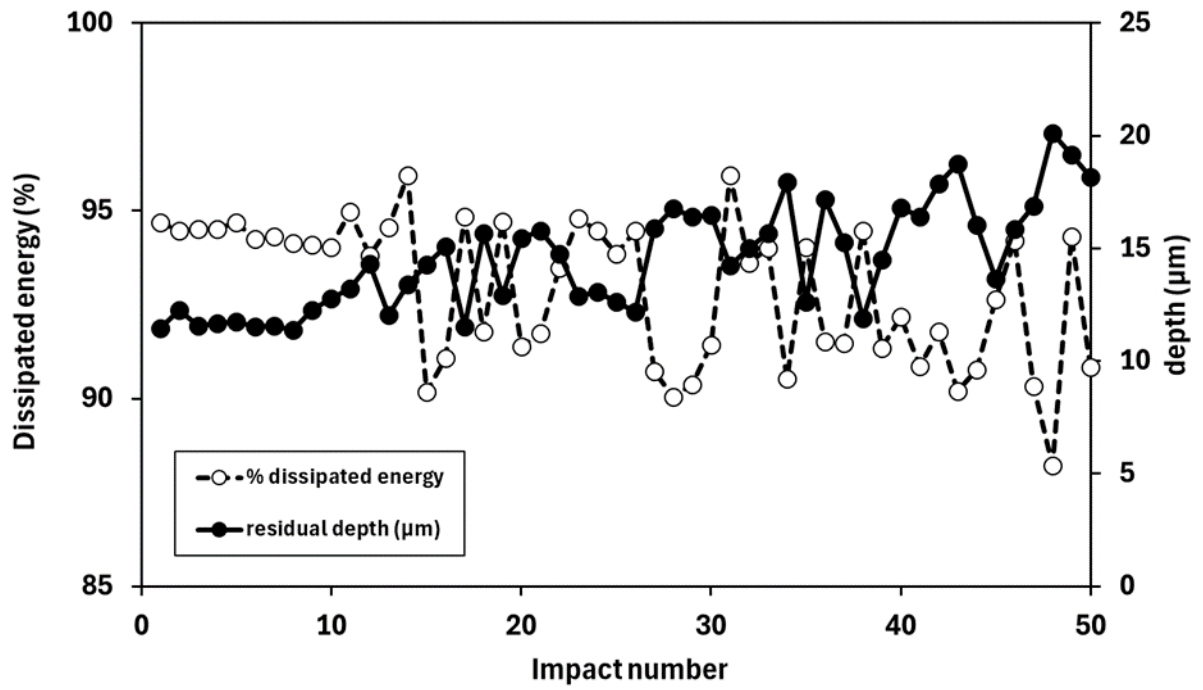
6(d,e)



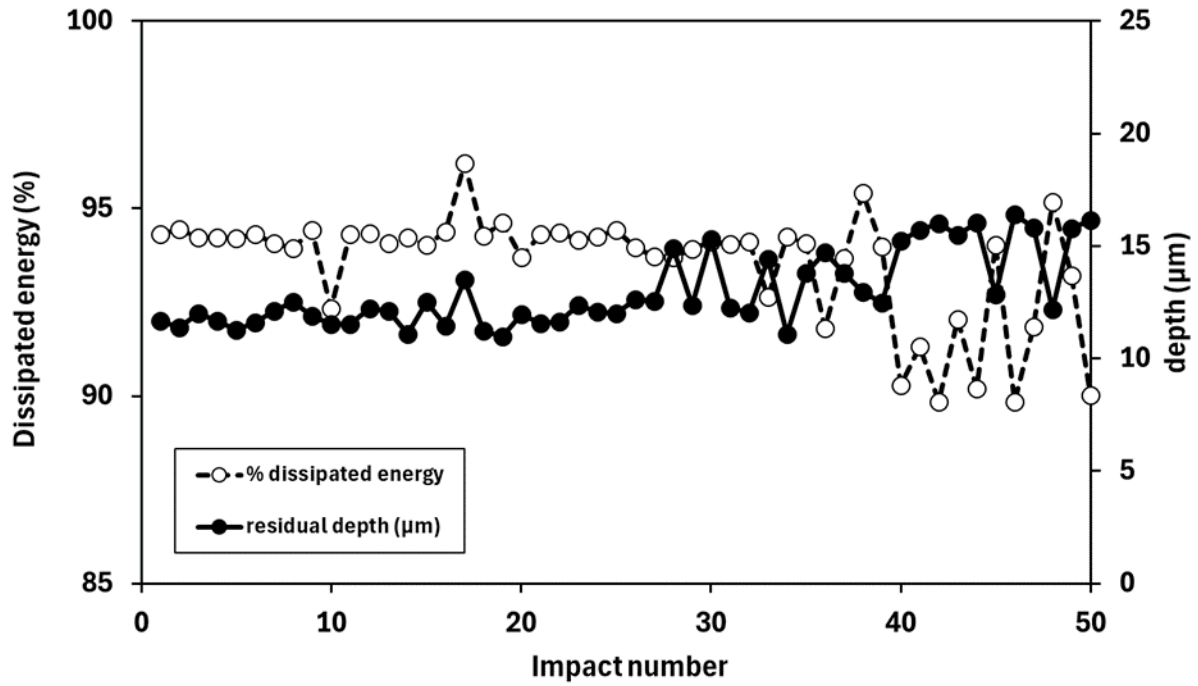
6(f)



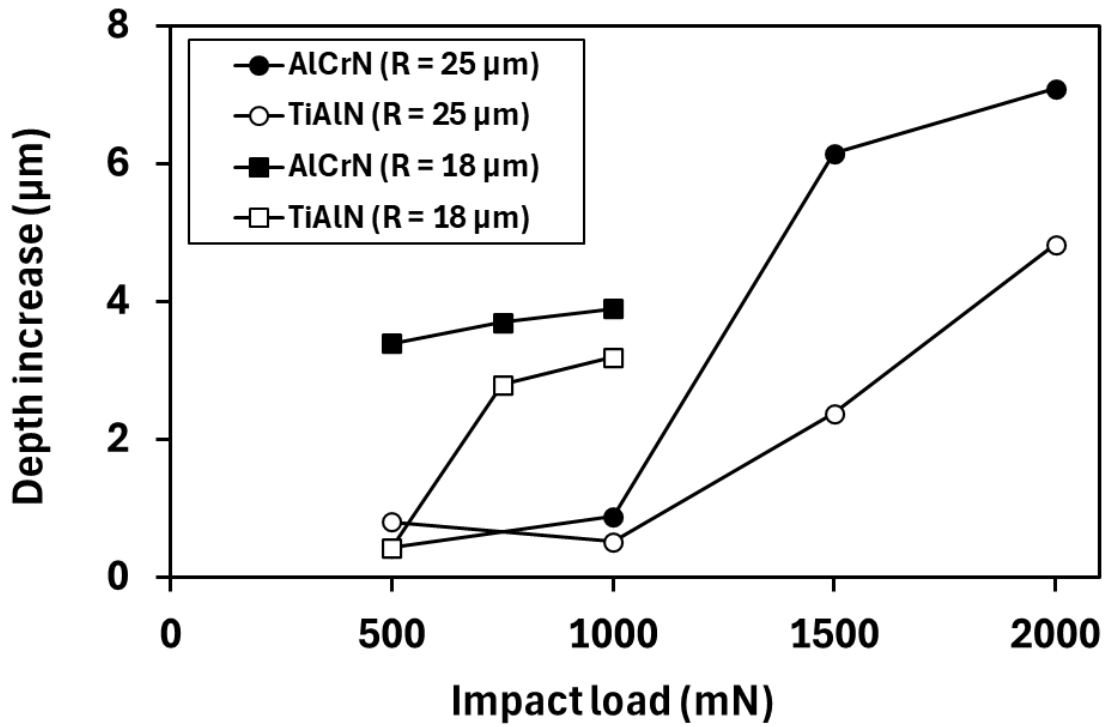
6(g)



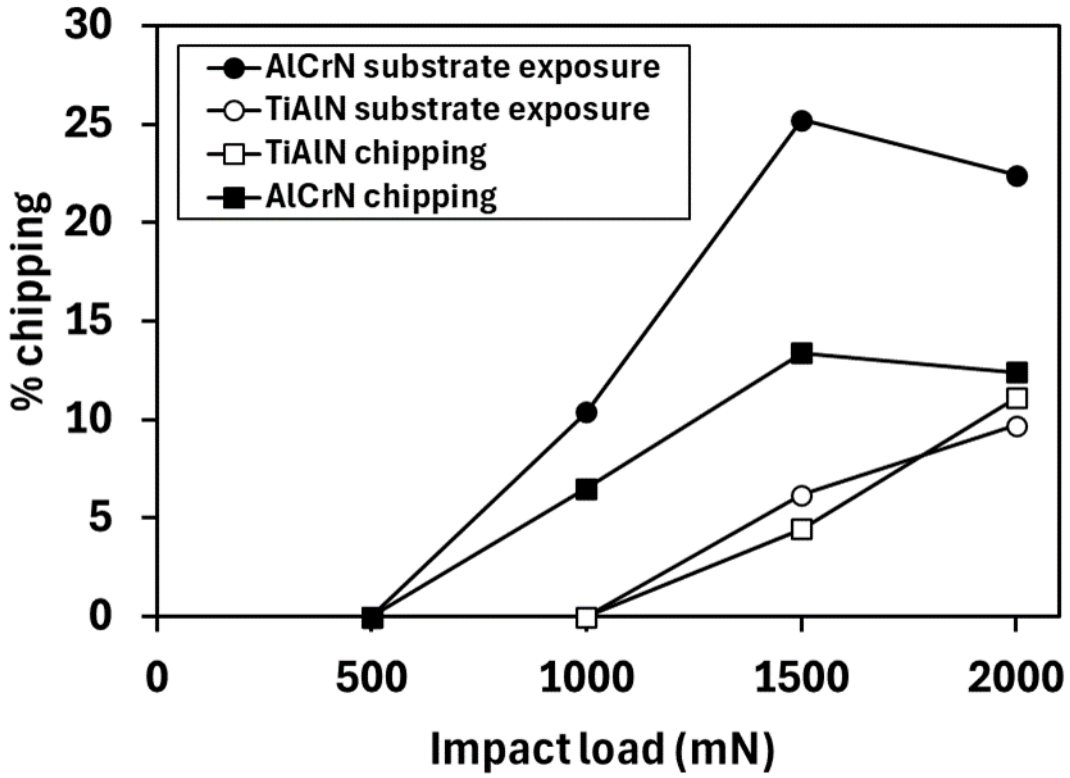
7(a)



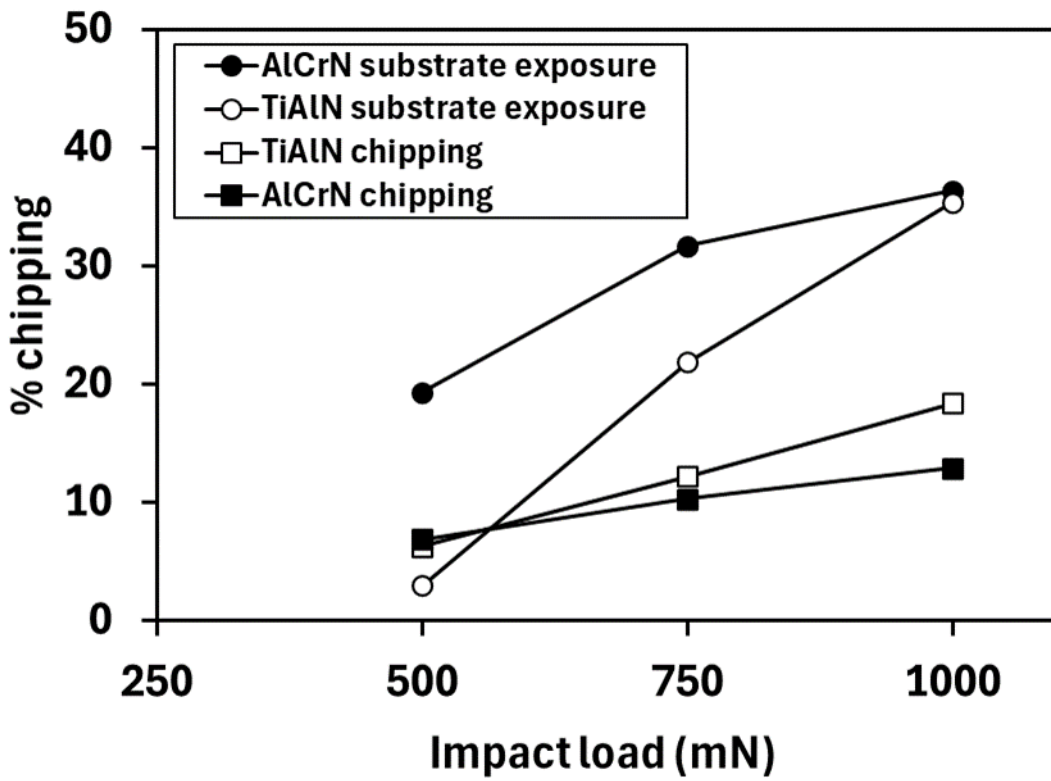
7(b)



8



9(a)



9(b)